Design and Fabrication of a Test Apparatus for Lightweight Flexible Space Modules for Assembly

by

Andrew R. Harlan

Submitted to the Department of Mechanical Engineering
in partial fulfillment of the requirements for the degree of

Bachelor of Science in Mechanical Engineering

at the

Massachusetts Institute of Technology

May, 2007

[June 2007]

Signature of Author: _____

Department of Mechanical Engineering
May 1, 2007

Certified by: _____

Steven Dubowsky
Professor of Mechanical Engineering
Thesis Supervisor

Accepted by: _____

John H. Lienhard V
Professor of Mechanical Engineering
Chairman, Undergraduate Thesis Committee

Design and Fabrication of a Test Apparatus for Lightweight Flexible Space Modules for Assembly

by

Andrew R. Harlan

Submitted to the Department of Mechanical Engineering
on May 1, 2007, in partial fulfillment of the
requirements for the degree of Bachelor of Science in
Mechanical Engineering

ABSTRACT

Future space missions will require the on-orbit construction of large structures, such as solar arrays and telescopes. Currently, on-orbit construction and maintenance work is primarily accomplished by astronauts, during extra-vehicular "space walks". These are expensive and pose risks to the astronauts' lives. In the future, it is expected that an increasing number of on-orbit construction missions will be performed by autonomous robotic systems. Large structures will be constructed using modules made of lightweight materials, and will be very flexible. In MIT's Field and Space Robotics Lab (FSRL), algorithms are being developed to optimize the transportation and assembly of large, flexible structures. To test these algorithms, it is necessary to have laboratory flexible beam modules with similar properties to structural space modules.

This thesis presents a design for a set of flexible modules which have comparable properties to proposed space modules. These modules are designed to be manipulated by a team of laboratory robots. The design process and final design of the flexible beam, which comprises a majority of the flexible module is presented. Several gripping devices, which attach the modules to robot manipulators, are also designed.

Thesis Supervisor: Steven Dubowsky

Title: Professor of Mechanical Engineering

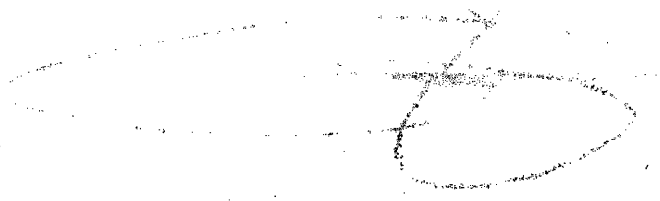

ACKNOWLEDGEMENTS

First, I would like to thank the Japan Aerospace Exploration Agency (JAXA) for their support of this research. I would also like to thank Dr. Steven Dubowsky and the members of the Field and Space Robotics Laboratory for their help and support throughout the course of this thesis. In particular, Peggy Boning and Hiro Ono for taking the time to make sure my work was up to par, and that I was always looking in the right direction. Finally, I could not be the person I am today without the extended support from my family and friends throughout my stay here at MIT.

CONTENTS

FIGURES

TABLES

CHAPTER

1

INTRODUCTION

1.1 Motivation

There is significant interest in building large space structures for use as telescopes, solar collectors, and other applications [3]. Launch technology limits the maximum payload that may be placed in orbit on a single trip. This requires on-orbit construction and assembly of these large structures.

It is important that safe and cost-effective methods are developed for on-orbit structure construction and assembly. Current on-orbit construction can only be performed by astronauts during extra-vehicular activity (EVA). These operations are dangerous, expensive, and time consuming. During the 2005 fiscal year, NASA allocated nearly 125 million dollars towards extra-vehicular activity systems [2]. For large scale construction missions, many tasks performed are simple, repetitive, and are well suited for autonomous robotic systems [3, 7, 10, 11, 12, 13].

An example is the assembly of a large space solar power plant (SSP) [1]. Current launching technology limits the size of arrays sent into Earth orbit. The largest solar array in orbit is connected to the International Space Station (ISS), as seen in Figure 1.1 [5].

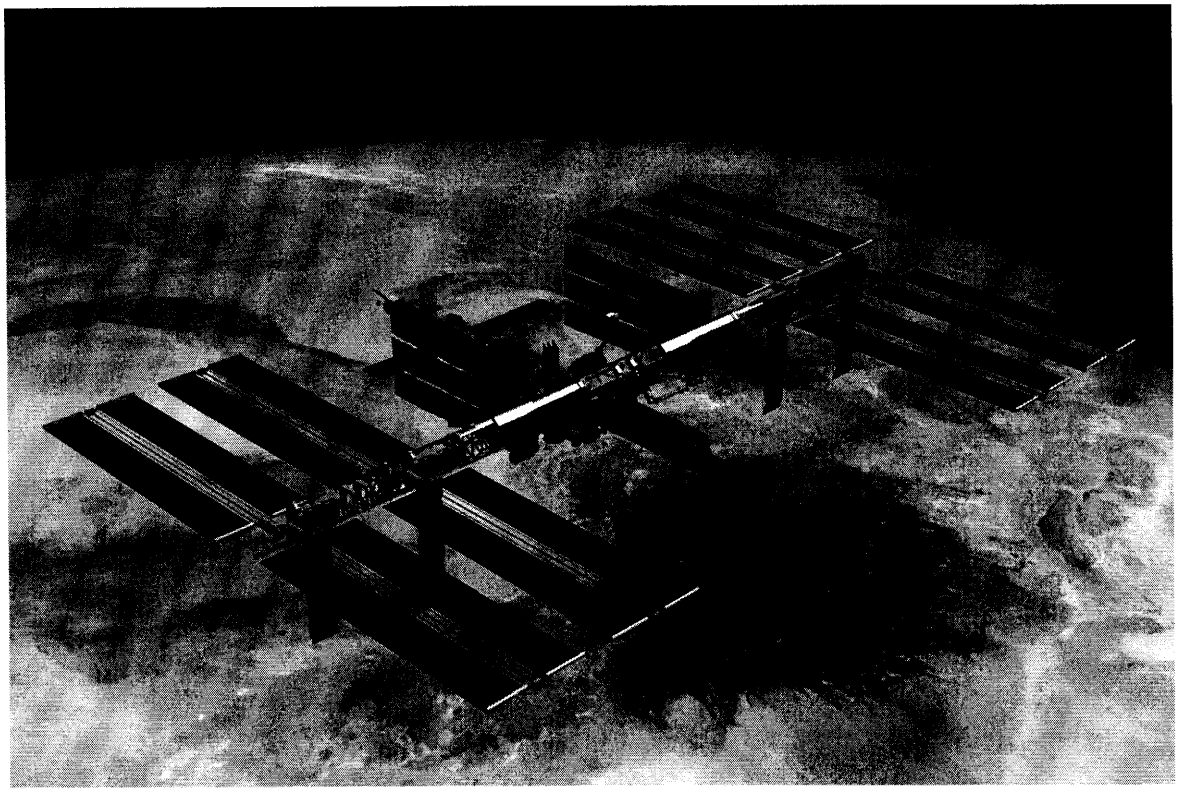

Figure 1.1. The International Space Station (ISS) is composed of many smaller pieces, assembled on-orbit. In this NASA concept rendering, all eight solar array pairs can be seen. [8].

The array is comprised of eight identical 33-meter panels, launched into orbit in sets of two. Only four of the eight panels have been attached. When fully completed, the solar arrays will cover an area of approximately 0.03 km^2 [5].

The large solar collectors for future SSP's would need many more modules. These SSP's are projected to require dozens to hundreds of modules, launched separately, then assembled in space [3]. Figure 1.2 shows a concept for a large 4 km^2 solar collector.

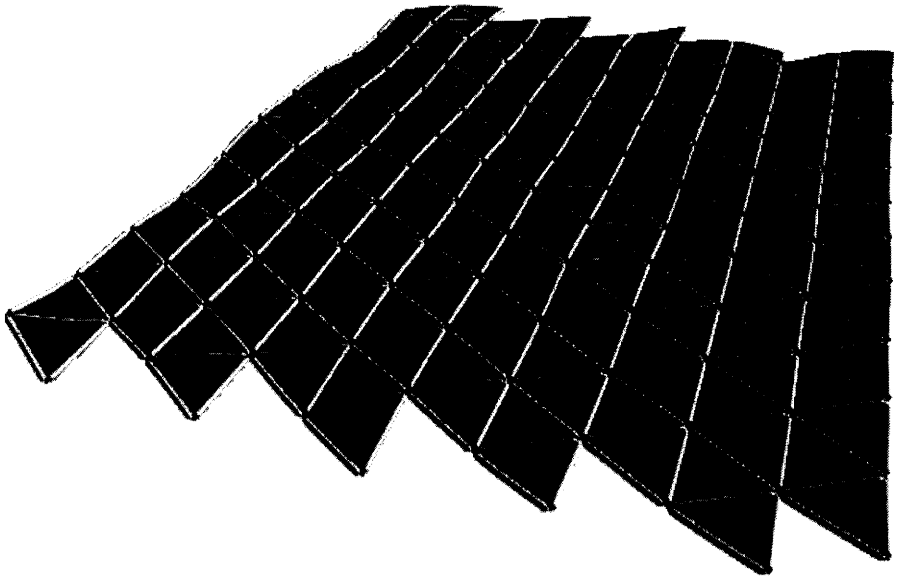

Figure 1.2. Concept for a 4 km^2 orbiting solar array power station [1, 4].

This structure would be composed of hundreds of identical modules, requiring repetition of assembly procedures. Figure 1.3 shows a concept for how this type of structure could be assembled by teams of autonomous robots.

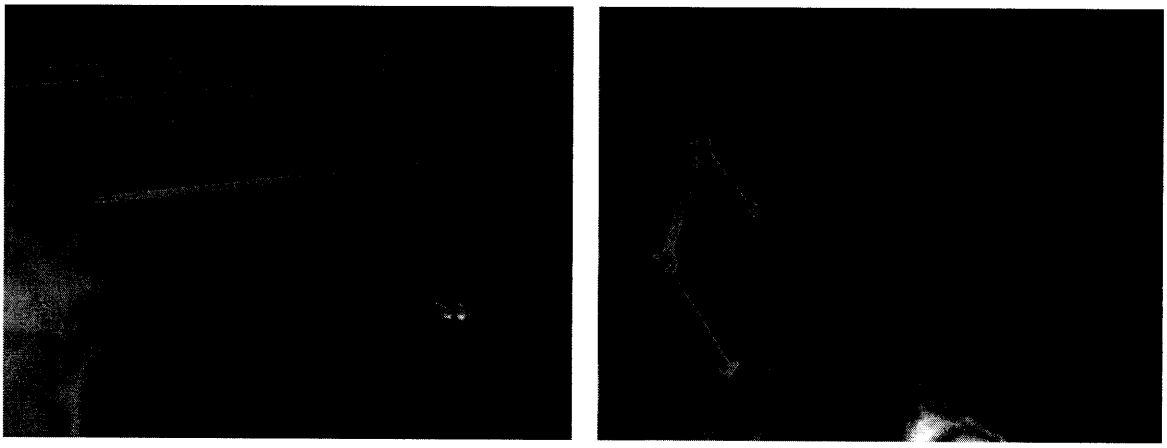

i) *ii)*

Figure 1.3. Possible scenario for transportation and assembly of structural elements for a solar array. Figure i) shows teams of robots transporting structural elements. Figure ii) shows multiple elements being connected [1].

In addition to size limits, current launch technology also imposes limits on the weight of objects that may be launched as payloads. The use of lightweight materials would minimize the number of launches, and hence, launch costs. However, the resulting support structures would be very flexible [3]. Transporting and assembling these large, flexible structures efficiently and without inducing substantial vibrations is a challenging task. This is a topic of research at MIT's Field and Space Robotics Lab (FSRL), a division of the Department of Mechanical Engineering. Control algorithms for large space structure assembly are being developed, but require experimental validation.

To test these transportation and assembly methods and algorithms, an experimental testbed is being constructed. This thesis focuses on the design and fabrication of flexible modules for this experimental testbed.

1.2 Approach and Outline of Thesis

This thesis consists of a study of flexible beams, and the design and testing of a series of flexible modules that can be transported and assembled by robots in the FSRL experimental system. This thesis is comprised of five chapters. This chapter presents the motivation and background for the thesis. Chapter 2 details requirements and objectives the design must meet. Chapter 3 describes the process of design and how a final design was achieved, and Chapter 4 highlights the features of the final design. A summary and proposal for future work concludes the thesis in Chapter 5.

CHAPTER

2

DESIGN OBJECTIVES AND SPECIFICATIONS

This chapter details the experimental background, constraints, and objectives from a design perspective.

2.1 Experiment Background

The core of the experimental testbed is a team of robots which support a flexible beam. These robots glide on a flat surface using set of air bearings, allowing them to translate and rotate within the horizontal plane. Figure 2.1 shows an overhead diagram of a pair of robots supporting a flexible beam.

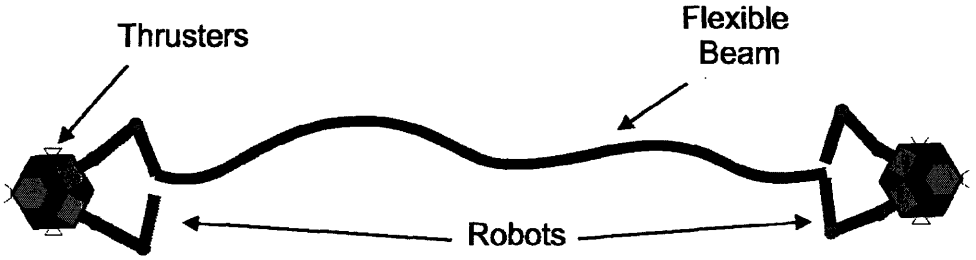

Figure 2.1 An overhead schematic of a pair of robots supporting a flexible beam.

By using different configurations of robots and beams, many different experiments can be performed. Figure 2.2 shows a more complex arrangement of robots with a passive floating module.

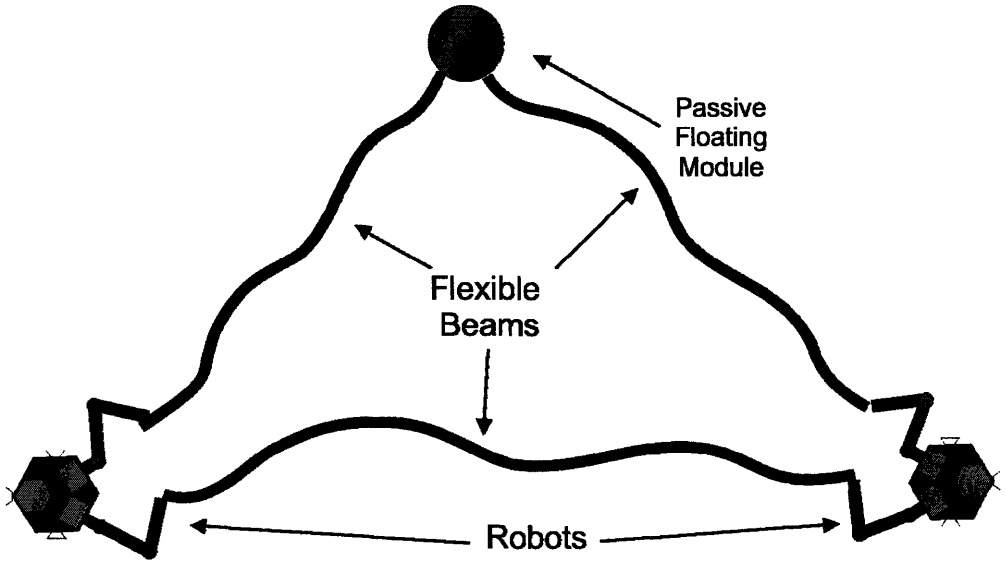

Figure 2.2 A more complex configuration with three beams, two robots, and one passive floating module.

The passive floating module is similar to a robot, except that it has no thrusters or manipulator arms. It is used only as a structural support. This thesis is concerned with the design of the flexible beam and all supporting hardware that allows it to interface with the robots.

2.2 Design Constraints

The design of the experimental beam must be compatible with existing robots and testing facilities. Many of the decisions made for the beam design were influenced by the capabilities of the experimental testbed, particularly by the capabilities of the robots used in the experiments. These capabilities include locomotion, manipulation, and sensing.

2.2.1 The FSRL Experimental Testbed

Simulation of a microgravity environment is accomplished by using the Microgravity Robotic System Testbed (MRST) in the MIT Field and Space Robotics

Laboratory. The system consists of a rectangular granite surface plate and a set of robots and passive modules that float on the surface plate.

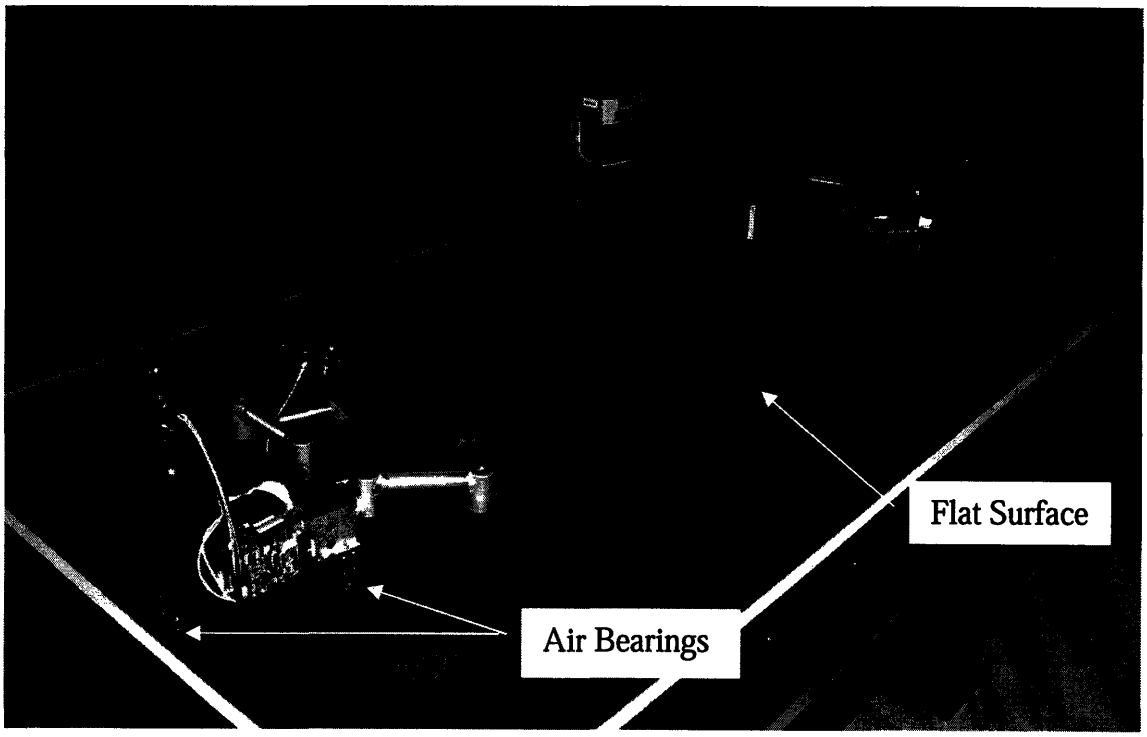

Figure 2.3 The Microgravity Robotic System Testbed located in the FSRL [FSRL stock photo].

The large granite slab serves as the foundation for the experimental setup. The granite slab is approximately 2.2 meters long by 1.3 meters wide. The surface is highly polished for consistent smoothness. It has also been leveled to ensure that gravitational effects do not cause any floating objects to drift.

Each floating object, whether robot or passive floating module, is equipped with a set of three low-friction porous air bearings. These bearings can be adjusted to ensure the platform they are supporting is level. The air bearings run on compressed carbon dioxide, which is stored in a tank on-board the robots and passive floating modules.

In addition to testing on the MRST, experiments are also intended to be performed in the Space Systems Laboratory, in MIT's Department of Aeronautics and Astronautics. This laboratory has an epoxy floor that has similar properties to the MRST, but is much larger. Its surface forms a 5 meter diameter hexagon, and is useful for performing experiments with longer beams and larger teams of robots.

2.2.2 Locomotion

The robots maneuver by using a set of compressed air thrusters. The thrusters are powered by the onboard carbon dioxide tanks, and have been designed to provide 0.1N of force each under full loading. Each robot is equipped with eight thrusters in orientations designed to control translation and rotation.

2.2.3 Manipulation

As shown in Figure 2.4, each free-floating robot is equipped with a pair of manipulator arms mounted in front of the robot.

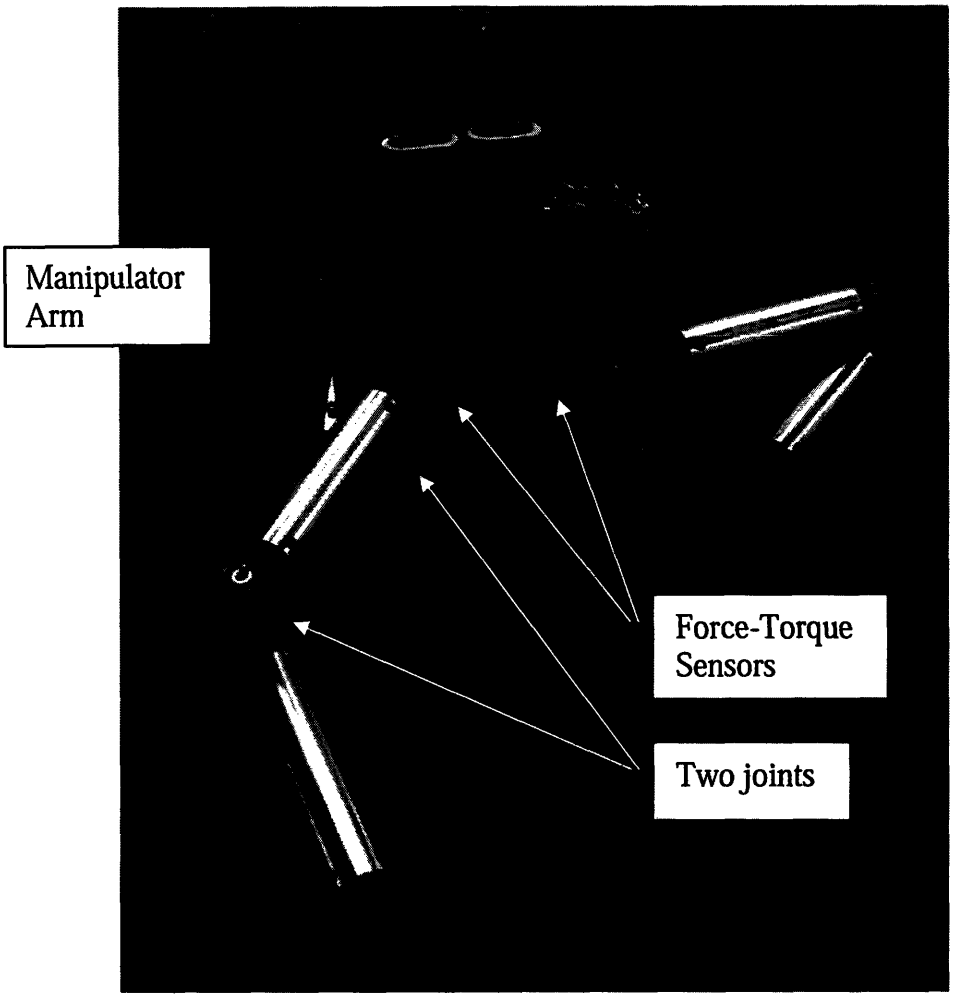

Figure 2.4. Each robot is equipped with pair of manipulator arms, mounted to force-torque sensors [FSRL stock photo].

Each manipulator consists of two links, and has two degrees of freedom in the plane parallel to the surface of the table. Each joint is equipped with a motor, as well as an optical shaft encoder for closed-loop feedback control. A force-torque sensor with a set of four strain gauge load cells is mounted at the base of each manipulator for measuring the forces and torques applied by the manipulator.

The force-torque sensors place limits on the force that the manipulators can support at their ends. The maximum force that can be supported out of the plane of the

table without damaging the sensors is estimated to be 250 grams. Therefore, a pair of robots can support a total weight no larger than 500 grams.

2.2.4 Sensing

Experiments may require that the beam support several measurement components. These components are used to track the position, velocity, and acceleration of the beam. They may add significant weight to the beam.

A camera mounted above the table can measure the position of the beam by locating fiducial markers attached along the length of the beam. These markers are made out of foam core, and add little weight to the beam. Figure 2.5 shows a possible configuration.

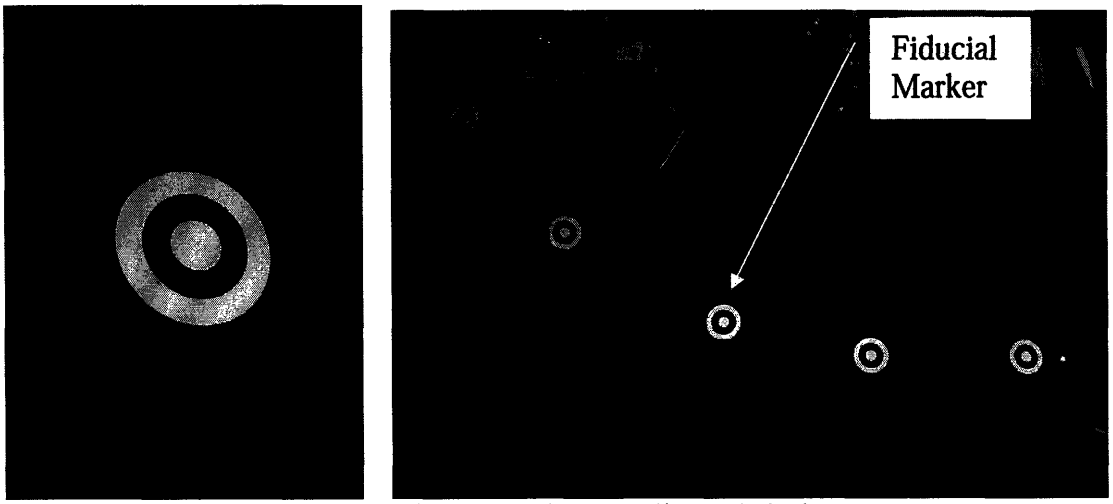

Figure 2.5. Fiducial markers can be mounted to visually track the beam's position over time.

Control algorithms used to transport the beams may also require accelerometers to be mounted along the length of the beam. Figure 2.6 shows an experiment performed by Amy Bilton of the FSRL, which involved a beam with accelerometers attached.

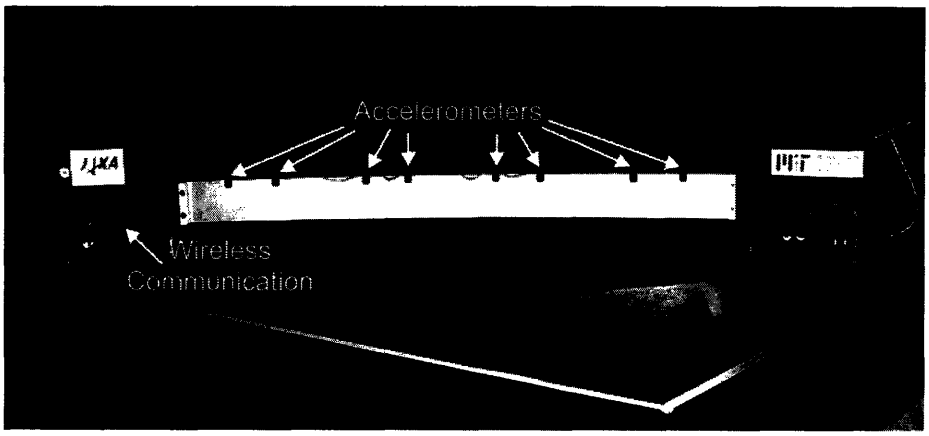

Figure 2.6. Accelerometers can be used to measure beam motion [1].

The smallest measurement that a single accelerometer used in this testbed can read is 5×10^{-5} g's. To obtain a meaningful reading, the minimum desired acceleration measurement should be at least one order of magnitude higher than this value. This limits the smallest acceleration range, therefore the lowest natural frequency which can be measured.

Another constraint is the robot control loop. The controller assumes that the frequencies of the dominant modes of vibration are much lower than the bandwidth of the control loop. This places an upper bound on the frequency of the first flexible mode of vibration, which is the most dominant mode.

2.2.5 Size Requirements

The size of the beam is limited by the table and flat floor size. On the small MRST table, two configurations are possible for transporting a long beam. Figure 2.7 illustrates these two configurations.

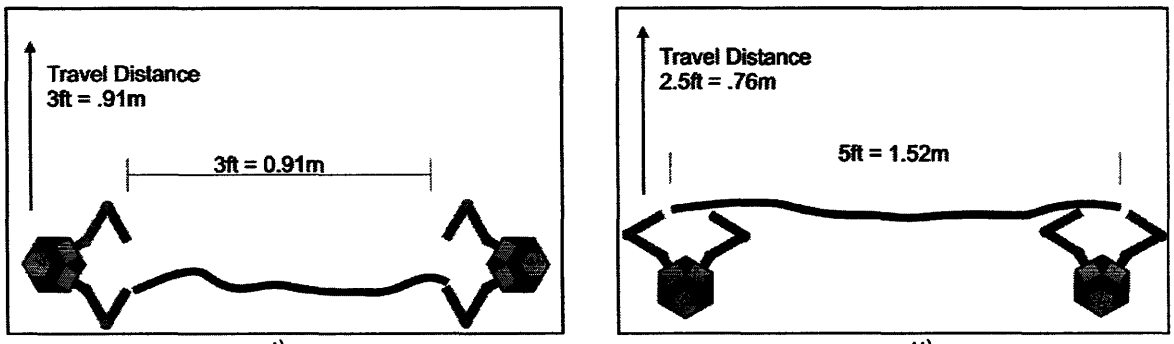

Figure 2.7. A scaled drawing of two options for transporting a beam on the MRST.

In Configuration i), two robots face each other across the long end of the table. A 0.91 meter beam is held between the two robots, and they transport it across the short side of the table. A second option is to place both of the robots in the same orientation facing the direction of travel, then span the beam from the furthest manipulator of each robot, as shown in Configuration ii). This orientation allows for a 1.52 meter beam. Configuration i) allows for a longer travel distance, but a shorter beam. Configuration ii) allows a longer beam, but less room for transportation.

2.3 Experiment Description

While the flexible modules can be used to test many different operations in a laboratory, for this thesis, the design of the flexible modules is focused on two different algorithm tests called transportation and assembly tests. Each experiment has different requirements for the flexible module assembly.

2.3.1 Transportation

The goal of the transportation experiment is to demonstrate and evaluate control algorithms that minimize the amplitude of vibration induced when a beam is moved from

one location an orientation to another [3]. The beam is transported by applying a force at both ends in a direction perpendicular to the axial dimension, as shown in Figure 2.8.

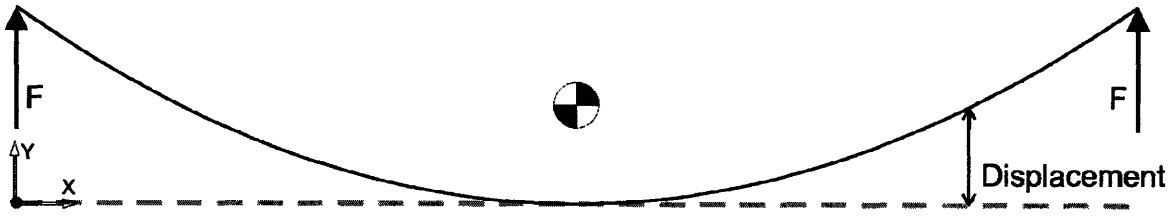

Figure 2.8. A force located at both extremities of the beam, perpendicular to its long axis will induce the largest deflections.

Because of the beam's flexibility, the forces shown above cause large transverse vibrations. Being able to visually see the beam deflection and vibration is essential for demonstrating the effectiveness of control algorithms.

In the transportation experiment, the beam is carried by two robots, one at each end of the beam. Each robot holds its manipulators rigidly and uses its thrusters to transport the beam[1]. A pin joint at the connection between the beam and each robot manipulator prevents the robots from applying moments to the beam in the plane of vibration. In this experiment, the robots contribute a significant end mass, which must be considered in the beam's dynamic model.

2.3.2 Assembly

The assembly experiment has different requirements for its flexible module. The goal of the assembly experiment is to demonstrate flexible space structure assembly control algorithms [3]. A team of robots will form a polygon by supporting several beams in a ring, see Figure 2.9.

[1] During further testing, the robots will used specialized algorithms to control the beam, at which point their manipulators are no longer locked. However, the dominant design criteria for this thesis is to determine a module which can achieve baseline results for comparison.

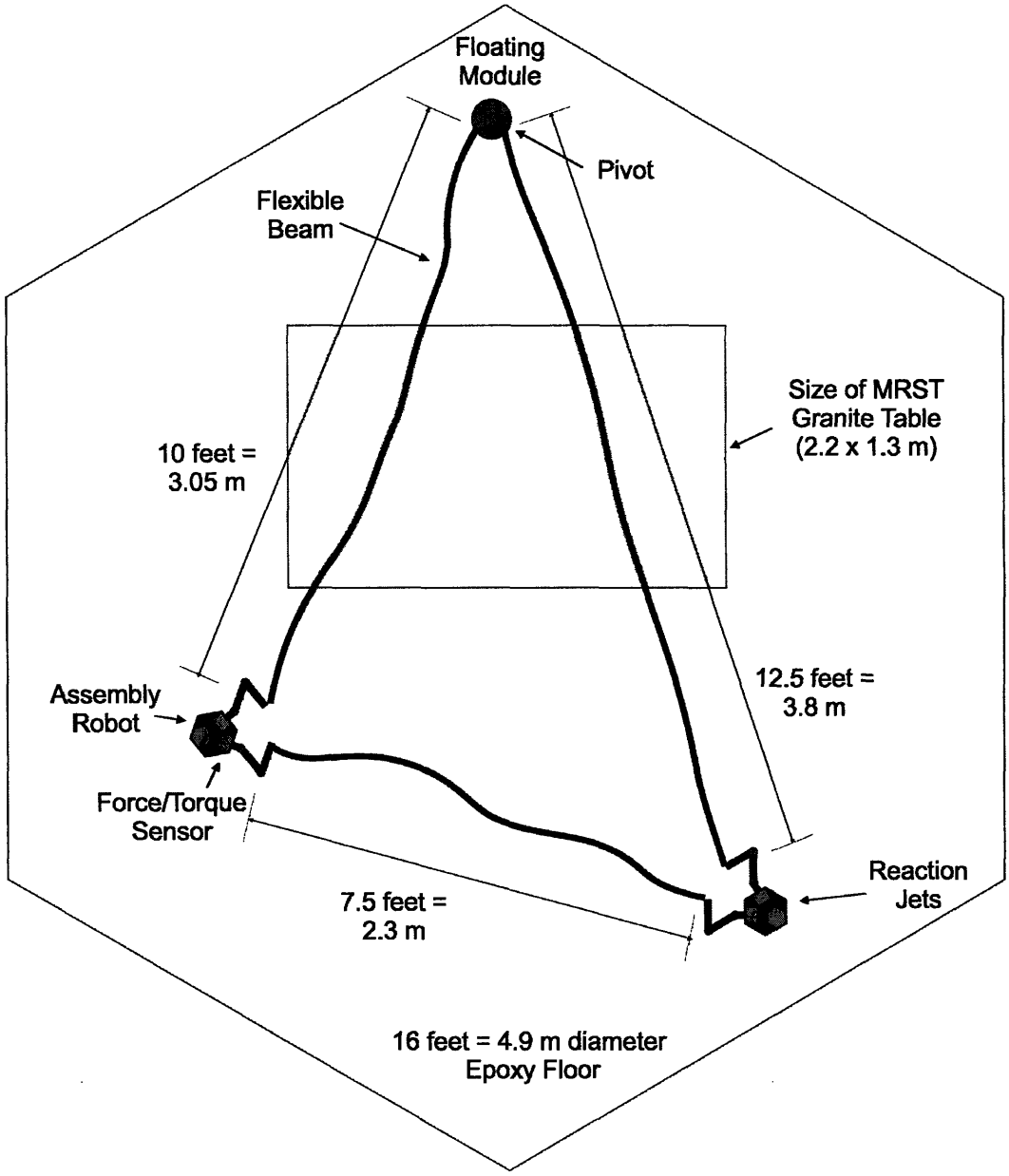

Figure 2.9. Scaled layout of an assembly experiment on a 5m diameter hexagonal floor [Peggy Boning, FSRL].

Each vertex of the polygon is either a robot or a passive floating module which has no active control. A passive floating module is a base with air bearings and two pin joints to connect beams. The experiment will be performed with the robots holding the beams in arbitrary orientations. When the experiment begins, the robots will bring all beam vertices into contact, forming a polygon. When space robots perform fine

assembly operations, they must be careful not to induce vibrations that would prevent assembly or cause collisions that could damage the system.

The assembly experiment is dynamically different from the transportation experiment because the robots do not undergo large translations. They remain in essentially the same location, and use their manipulators to reposition the beams. Because the robots are not undergoing significant translations, their mass is no longer considered in the vibration dynamics of the beam.

The baseline case involves the robots bringing their manipulators together in a quick, straight line. Once baseline results are achieved, different control algorithms will govern how the robot manipulators behave. Results will then be compared to the baseline case.

CHAPTER

3

DESIGN ANALYSIS AND PROCESSES

3.1 Prior Hardware

The concept for the mechanical design of the flexible structures evolved from prior experimental work in the FSRL. The robots which transport the structures were designed by Dr. Jamie Nichol. Two previous studies also required flexible beams to be constructed. In his Ph.D. thesis, Dr. Matt Lichter demonstrated vibration and mode shape estimation with vision sensors [4]. A flexible test beam was used for verifying results. More recently, Amy Bilton explored the fusion of remote vision and on-board acceleration data for her Master's thesis [1]. Her results were verified with an experimental system with a beam. This flexible beam design was used as a basis and benchmark for designs in this thesis.

Bilton's design used two passive floating modules to support the beam. Bilton's design obtained very large deflections by starting with the entire the structure in an initially deformed position. The weight of the beam was not of great concern in Bilton's experiments because it was clamped directly onto two passive floating modules, giving it stiff structural support. There was also less concern with obtaining a low natural frequency with the beam, because the beam was supported between two floating modules. The floating modules have large rotational inertias, which decrease the natural frequency of the system. This allowed Bilton to use a beam of greater height, which is

less susceptible to sag. In this work, manipulator arms are used to support the beam, and therefore the design must be more concerned with weight, beam sag, and natural frequency.

3.2 Materials

In the selection of a material for one of the flexible beams, three materials were considered: aluminum, stainless steel, and uniaxial carbon fiber. These three materials were considered because of their availability, their material properties, and their low cost.

The aluminum considered was 6061-T651. It was chosen for its low stiffness, light weight, and corrosion resistance. The choice for stainless steel was A304. This material was chosen for its low damping, resistance to corrosion, and its prior use in Bilton's experiments. The third choice for material was uniaxial Magnamite AS4C carbon fiber. This material was chosen for its high torsional stiffness, low bending stiffness, and light weight.

While the material properties of aluminum and stainless steel are simple and well known, the properties of the carbon fiber material are non-isotropic. The carbon fiber beam is mounted so that the individual fibers run vertically, out of the plane of the table. This results in a high torsional stiffness and moderate axial stiffness. Since the in-plane bending of this beam does not cause stress in the direction the fibers, the beam stiffness is based on the modulus of elasticity of the resin that binds the fibers together. This resin has a significantly lower modulus than the carbon fiber threads.

3.3 Beam Analysis

Analysis of the flexible dynamics of the beam was primarily performed using the MATLAB software package. A simple finite element method calculation was programmed and used to determine vibration characteristics as a function of the physical properties of the beam. MATLAB was chosen as the primary analysis technique over full finite element analysis packages such as ADINA, COSMOS, or Nastran because of its increased flexibility, rapid simulation rate, and ease of use.

3.3.1 Assumptions

The model used neglects the damping due to internal energy dissipation and air resistance from the motion of the beam. It also is assumes that the beam is supported perfectly perpendicular to the plane of the table, and does not suffer from any out-of-plane sag, which is discussed in Section 3.6.1. The robots holding the beam are modeled as point masses rigidly attached to each end of the beam. Since the end masses are modeled as point masses, their rotational inertia is not considered in the model. Overall, the beam is modeled as a free-free end condition one-dimensional beam, as seen in Figure 3.1.

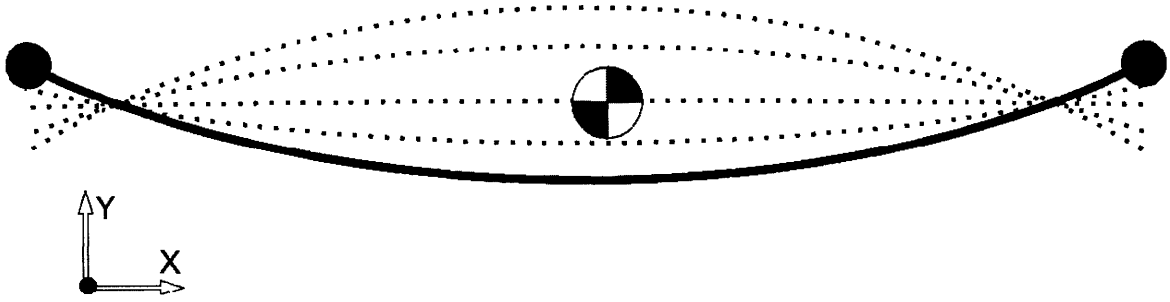

Figure 3.1. A free-free beam has no restraints or end conditions, vibrating freely about its center of mass.

3.3.2 Vibration Analysis

To simulate the flexible beam, the model is divided into a series of finite elements, each with its own dynamics. Modeling interactions between individual elements produces a larger model reproducing the entire beam's dynamics. The connection between each element is often referred to as a node. Unfortunately, vibration analysis also uses the word "node" for a different concept. To avoid confusion, this thesis uses the word "joint" to refer to the connection between two elements.

A long beam can be subdivided into a set of discrete elements. Figure 3.2 shows a single, one dimensional element.

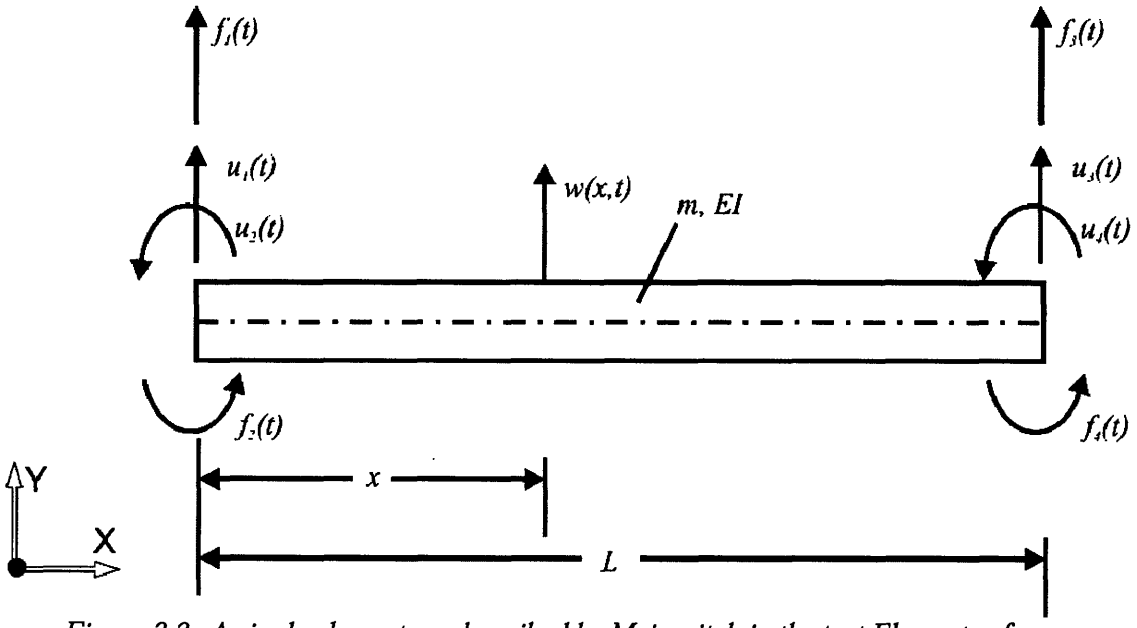

Figure 3.2. A single element, as described by Meirovitch in the text Elements of Vibration Analysis [6].

A more complex beam can be described by using several elements. Figure 3.3 shows how a single beam can be represented by three elements.

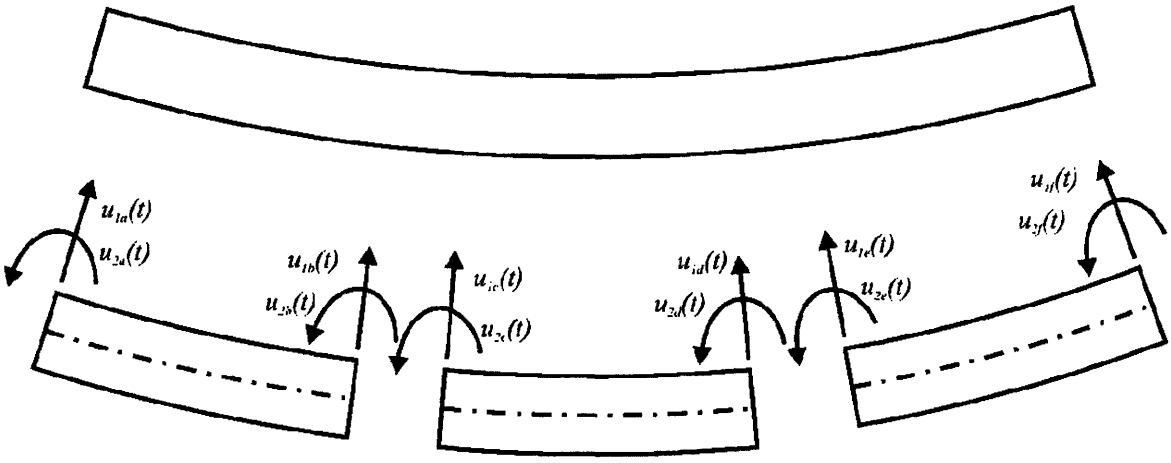

Figure 3.3. A flexing beam divided into three elements.

In order for the elements to act as a single body, they must have matching end conditions. In the picture above, $u_{1b}(t) = u_{1c}(t)$. Other end conditions match in the same manner. Finite element models may be divided into as little as two elements, or as many as millions of elements. Increasing the number of elements increases the accuracy of the vibration model, especially at higher modes. However, this also increases the time and complexity of calculation [6]. Since the dynamics of this system primarily involve the first mode of vibration, a large number of elements is not necessary. In this thesis, all finite element calculations divide the beam into 12 equal segments, which returns an acceptable amount of accuracy.

This study simulates beam deflections by using well-known Lagrangian analysis, as described by Meirovitch in the text *Elements of Vibration Analysis* [6]. A brief summary is shown here. A single, one dimensional element is shown in Figure 3.2 to illustrate the analysis.

The element is of length L, has a constant mass per unit length, m, and a uniform stiffness EI, where I is the second moment of inertia about the neutral axis in the bending plane and E is the modulus of elasticity of the beam material. The translational and

rotational displacements of the beam ends are described by $u_i(x,t)$ as shown in Figure 3.2. These displacements each have associated joint forces and bending moments.

First, the definitions of kinetic and potential energy are defined along the length of the beam. The kinetic energy is

$$T(t) = \frac{1}{2}\int_0^L m\left[\frac{\partial w(x,t)}{\partial t}\right]^2 dx \tag{3.1}$$

and the potential energy is

$$V(t) = \frac{1}{2}\int_0^L EI\left[\frac{\partial^2 w(x,t)}{\partial x^2}\right]^2 dx \tag{3.2}$$

At each joint, the associated forces can be determined by applying the principles of virtual work. On the element described above, $f_1^*(t)$ and $f_3^*(t)$ represent forces applied at each respective end of the element by adjacent elements. Likewise, $f_2^*(t)$ and $f_4^*(t)$ represent moments applied by adjacent elements. $f(x,t)$ represents a distributed non-conservative force acting on the element. Virtual work can now be written as

$$\begin{aligned}\overline{\delta W} &= \int_0^L f(x,t)\,\delta u(x,t)\,dx + \sum_{j=1}^{4} f_j^*(t)\,\delta u_j(t) \\ &= \sum_{j=1}^{4} f_j(t)\,\delta u_j(t)\end{aligned} \tag{3.3}$$

where

$$
\begin{aligned}
f(t)_1 &= \int_0^L f(x,t)\left(1-3\frac{x^2}{L^2}+2\frac{x^3}{L^3}\right)dx+ f_1^*(t)\\
f_2(t) &= \int_0^L f(x,t)\left(\frac{x}{L}-2\frac{x^2}{L^2}+\frac{x^3}{L^3}\right)Ldx+ f_2^*(t)\\
f_3(t) &= \int_0^L f(x,t)\left(3\frac{x^2}{L^2}-2\frac{x^3}{L^3}\right)dx+ f_3^*(t)\\
f_4(t) &= -\int_0^L f(x,t)\left(\frac{x^2}{L^2}-\frac{x^3}{L^3}\right)Ldx+ f_4^*(t)
\end{aligned}
\tag{3.4}
$$

Lagrange's equation is defined as

$$
\frac{d}{dt}\left(\frac{\partial T}{\partial \dot{q}_j}\right)-\frac{\partial T}{\partial q_j}+\frac{\partial V}{\partial q_j}=Q_j \tag{3.5}
$$

Combining equations 3.1, 3.2, 3.3 into Lagrange's equation, 3.5, the result is

$$
[m]\{\ddot{u}(t)\}+[k]\{u(t)\}=\{f(t)\} \tag{3.6}
$$

where

$$
[m]=\frac{mL}{420}\begin{bmatrix} 156 & 22L & 54 & -13L \\ 22L & 4L^2 & 13L & -3L^2 \\ 54 & 13L & 156 & -22L \\ -13L & -3L^2 & -22L & 4L^2 \end{bmatrix} \tag{3.7}
$$

and

$$
[k]=\frac{EI}{L^3}\begin{bmatrix} 12 & 6L & -12 & 6L \\ 6L & 4L^2 & -6L & 2L^2 \\ -12 & -6L & 12 & -6L \\ 6L & 2L^2 & -6L & 4L^2 \end{bmatrix} \tag{3.8}
$$

The mass matrix is represented by $[m]$, and the stiffness matrix is represented by $[k]$. The vectors $\{u(t)\}$ and $\{f(t)\}$ are four-dimensional, and represent the

translational displacements, rotational displacements, forces, and torques previously defined in Figure 3.3.

3.4 Simulation

The mass and stiffness matrices described in Section 3.3.2 above were used in a MATLAB script written by Peggy Boning, FSRL. Given inputs such as geometry, loading conditions, and mass distribution along the beam, the script output mode shape, frequency, and maximum deflection information. To ensure the validity of the results, several identical cases were also evaluated in ADINA, finite element analysis software package, and the results were compared.

The results for natural frequency calculations from ADINA agreed to within 0.05% across five different lengths of beams. Figure 3.4 plots both results.

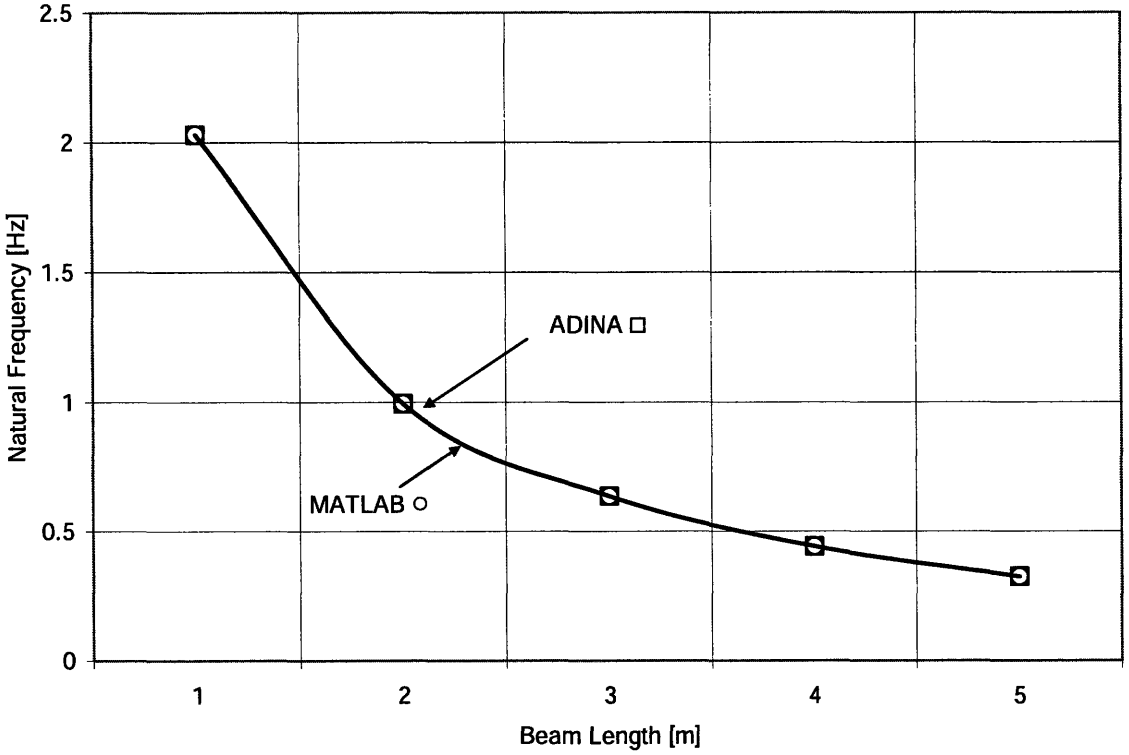

Figure 3.4. <0.05% variance between identical test cases using two different simulation packages to compute the first non-rigid natural frequency.[1]

3.5 Results

Following multiple design iterations, a final beam was chosen. Aluminum was selected as the material for the beam primarily because of its low modulus of elasticity. Large deflections are necessary in order to see visible results, and to obtain larger acceleration readings from accelerometers mounted on the beam. Simulation showed that aluminum beams have almost as low of a natural frequency as the steel beams, but weigh considerably less. Table 3.1 compares physical properties of identical beams composed out of different materials.

[1] The graphed natural frequencies do not reflect the final design choice. This data is collected from simulations of a beam of similar properties.

Table 3.1. Comparison of properties of a free-free beam 1.4 m long, 20 mm tall and 0.76 mm thick with no additional point masses.

	Weight	1st Mode Natural Frequency	Max Deflection
Aluminum	57.4 g	2.03 Hz	5.0 cm
Stainless Steel	170.0 g	1.95 Hz	1.8 cm
Carbon Fiber	37.8 g	3.57 Hz	2.5 cm

In the first two categories, weight and natural frequency, a lower result is more desirable. In the third category, maximum deflection, a larger result is better. Each beam material carries the most desirable value in one of the three main categories considered; however, the aluminum beam has the best overall average.

After a material was selected, the length, width, and height of the beam were chosen to meet design requirements. The selected dimensions are a height of 30 mm, thickness of 0.76 mm. The lengths match those described in Section 2.3.

3.6 Gripping Joint Design

In order to mount the beam on the robot, a gripping joint needs to be manufactured.

3.6.1 Design Requirements

The design of the gripper required a method of supporting the beam, while still providing a pin joint to allow the beam to rotate in-plane at the end of the robot manipulator. This ensures the robot is not applying any unwanted moments on the beam within the plane of the table surface. The pin joint needs to be low-friction yet remain very stiff to ensure that the beam does not flex out-of-plane. Figure 3.5, Diagram i)

shows the cross section of a beam remaining in-plane. Figure 3.5, Diagram ii) shows a beam sagging out-of-plane. Out-of-plane sag affects the vibrating dynamics of the beam, such that it can no longer be modeled as a two dimensional body. Figure 3.5 illustrates out-of-plane sag.

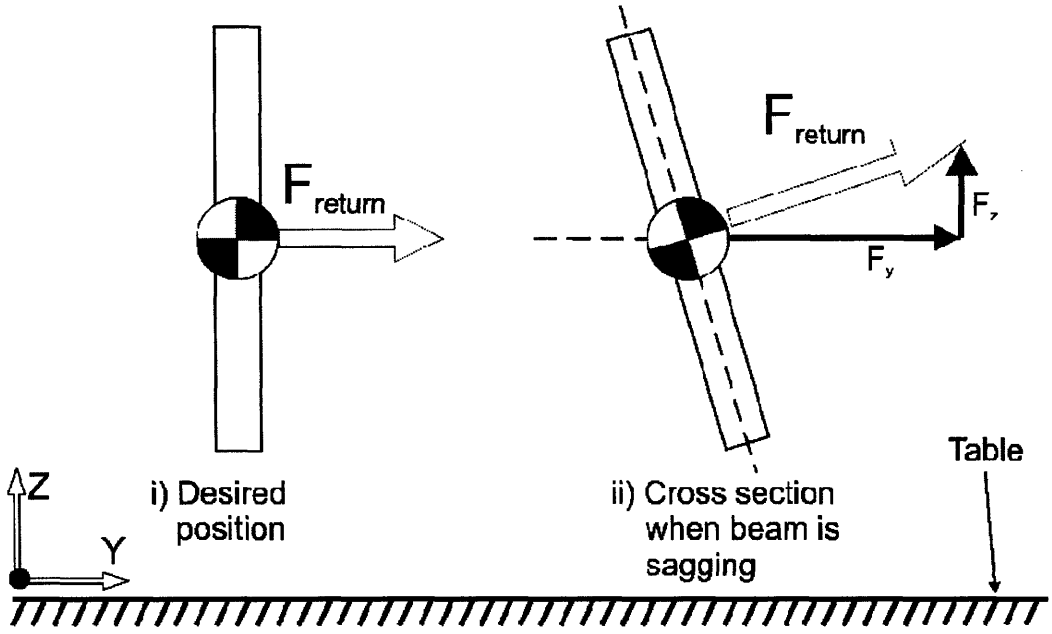

Figure 3.5. Cross-section of a beam during sag conditions. Return force F_{return} is partially out-of-plane, violating modeling conditions.

If the beam sags, the in-plane return force vector F_y is smaller than F_{return}. A component of F_{return} also points upward, lifting the center of mass of the beam.

When the beam sags out-of-plane, its center of mass also drops. This leads to a bi-stable situation in which the beam tends to come to rest in a curved position with some potential energy stored, rather than a straight position with no lost energy. To the observer, it looks as though the beam gets "stuck" in a curved position, unable to straighten itself. A slight tap on the beam and it may bounce back and forth between its current position and that of a curve mirroring its original, eventually coming to rest in one

of the two states. Raising the center of mass over this hump wastes energy, and causes the beam to vibrate in an irregular, non-planar manner. Every time the beam oscillates across the middle, it must expend stored energy to raise its center of mass over the "hump" in the middle. This motion can be likened to that of a ball moving back and forth on a curved W-shape track, as shown in Figure 3.6.

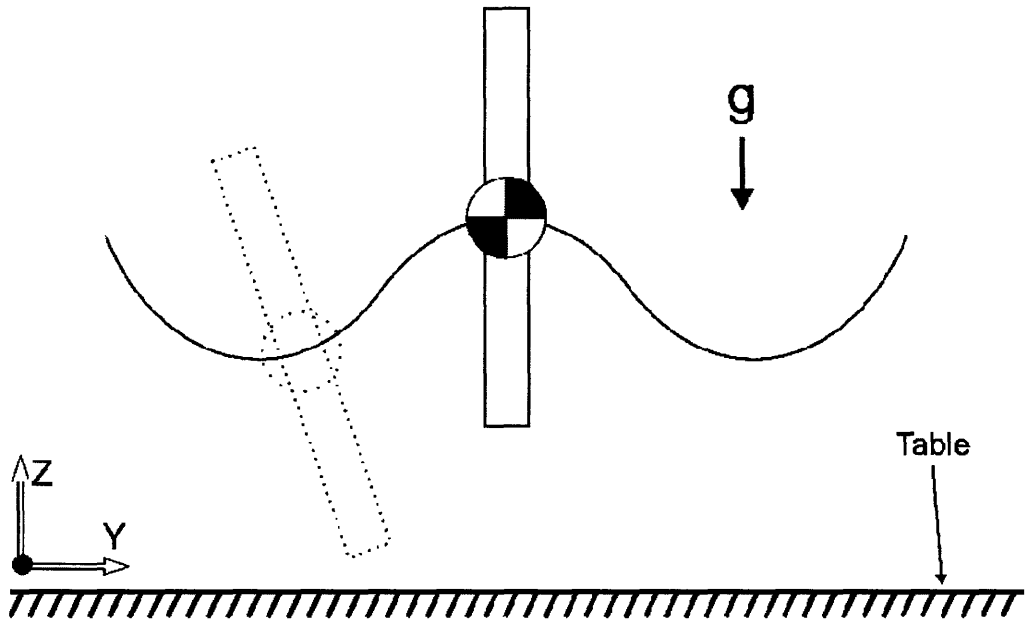

Figure 3.6. When the beam sags during vibration, its center of mass moves lower. This causes a bi-stable situation, visualized here as a potential field with two valleys.

The situation is bi-stable, rather than fully unstable because of the return force of the beam. As the beam extends farther away from the starting position, the return force eventually overcomes the effect of gravity, and a stable position is reached.

The gripper must also be lightweight. This helps keep the payload mass under the estimated maximum of 500 grams, and allows more flexibility in beam design choices.

3.6.2 Design Iterations

The general concept was to create a simple pin joint using few parts and remaining as simple as possible. The first design iteration used a single ball bearing around a vertically mounted pin. The pin was shouldered so that the weight of the beam was transmitted as a thrust load onto the bearing. The ball bearing was press-fit completely inside a piece of high density polyethylene (HDPE). This piece, dubbed the "hand piece" had a single screw which clamped through a hole in the beam. Figure 3.7 shows an isometric view of the overall design.

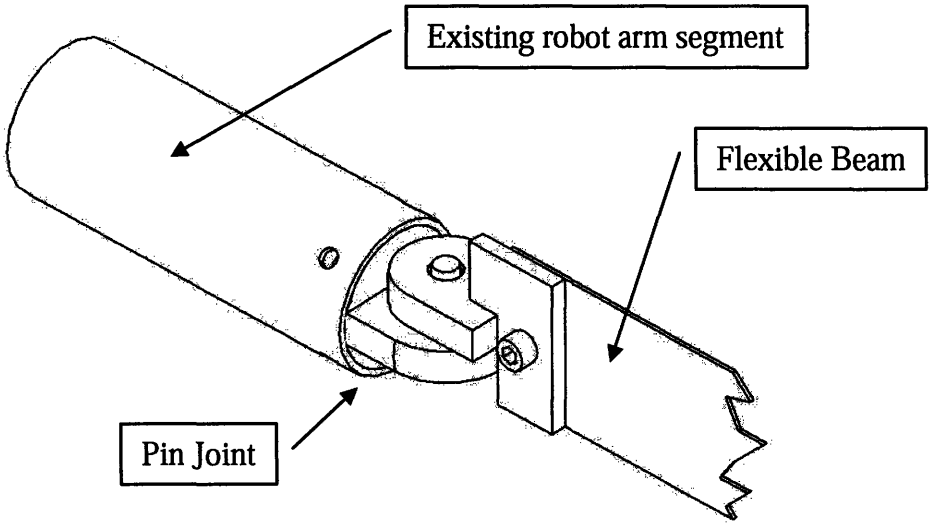

Figure 3.7. First gripper joint design.

The design has four custom designed pieces, labeled in Figure 3.8.

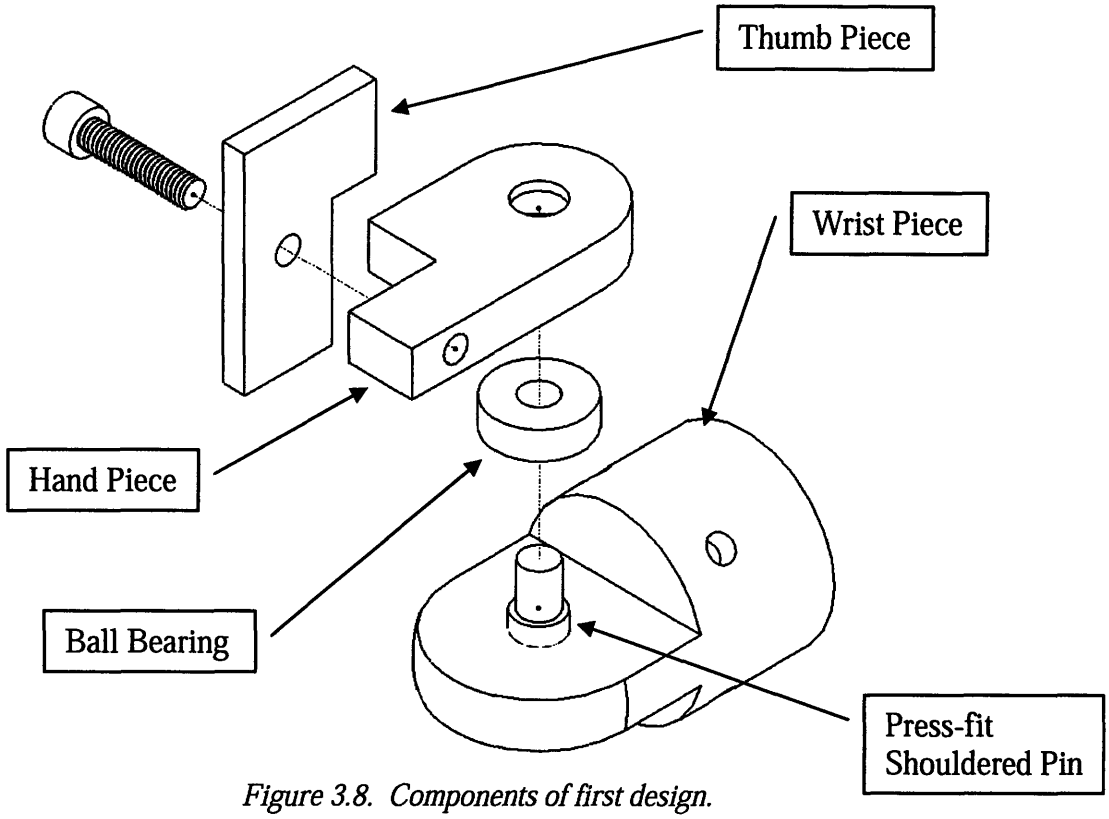

Figure 3.8. Components of first design.

The most substantial problem with this design was the large moment being transferred through the ball bearing. Initially, it was assumed that out-of-plane moments induced by the beam would be insignificant, and could be supported by the bearing. However, after constructing a prototype, sag was observed which visibly altered the vibration pattern of the beam.

To increase the stiffness of the joint against moments out of the plane, a second bearing was added in the final design. This bearing was placed approximately four pin-diameters above the first bearing. Section 4.2.2 outlines the final design.

CHAPTER

4

DESIGN

4.1 Beam Design

The final choice for beam material was Aluminum 6061. A primary factor in this decision was its low modulus of elasticity, allowing for larger beam deflections for a given force. The aluminum beam has a low natural frequency relative to the other materials considered, and is moderately lightweight. The final beam design has cross-section dimensions 0.76mm thick and 30 mm high.

4.1.1 Experimental Layout

The transportation and assembly experiments each placed different constraints on the beam. After modeling the transportation experiment, it was determined that the maximum force output on the thrusters would not provide adequate acceleration values at the ends of the beams to induce a visible deflection. A solution to this problem is to add a middle mass to the beam used in the transportation experiment. The addition of a third mass in the middle of the beam shifts the center of mass of the entire system, changing its dynamic properties, as shown in Figure 4.1.

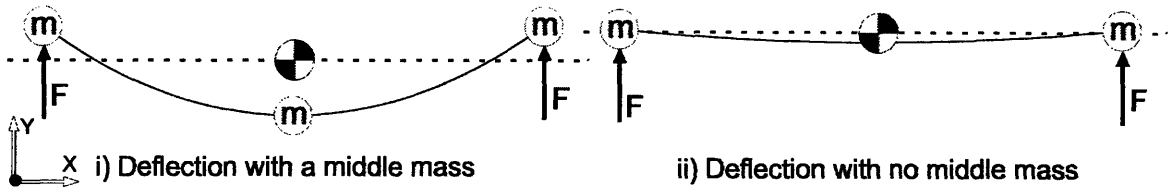

Figure 4.1 When a middle mass is added, larger deflections can be observed.

A center mass of approximately 2 kg gave the beam a much more visible deformation. Because of the significant weight of the middle mass, hanging the mass directly from the beam was not possible, for it would exceed the 500 gram limit that the robot manipulators could support.

Instead a passive support, modules such as the one used in the assembly experiment, were modified to clamp to the middle of the beam. This module is described in further detail in Section 4.3.

The assembly experiment is arranged in the same fashion as displayed previously in Figure 2.2. The fast motion of the robot arms, roughly 1 rad/s at each joint, induces a much quicker beam displacement than the transportation experiment. Since the mass of the robot no longer moves with the beam, a middle mass is not necessary to induce large deflections. The only details that have not been addressed involve the passive floating module. These are discussed in Section 4.3.

4.1.2 Beam Joints

One problem with using aluminum is that it must be purchased in sheets. The longest retail sheet that was readily available was 2.4 meters. However, a metal shear over 1.5 meters was not readily available. Attempting to buy sheet aluminum cut to size

in long strips was prohibitively expensive. Instead a jointing method was necessary in order to connect multiple smaller beams together into a single, continuous beam.

Each 1.5 meter flexible beam has two holes cut in each end. By overlapping the holes of two beams and using screws and nuts to fasten them together, a simple solution was reached, as shown in Figure 4.2

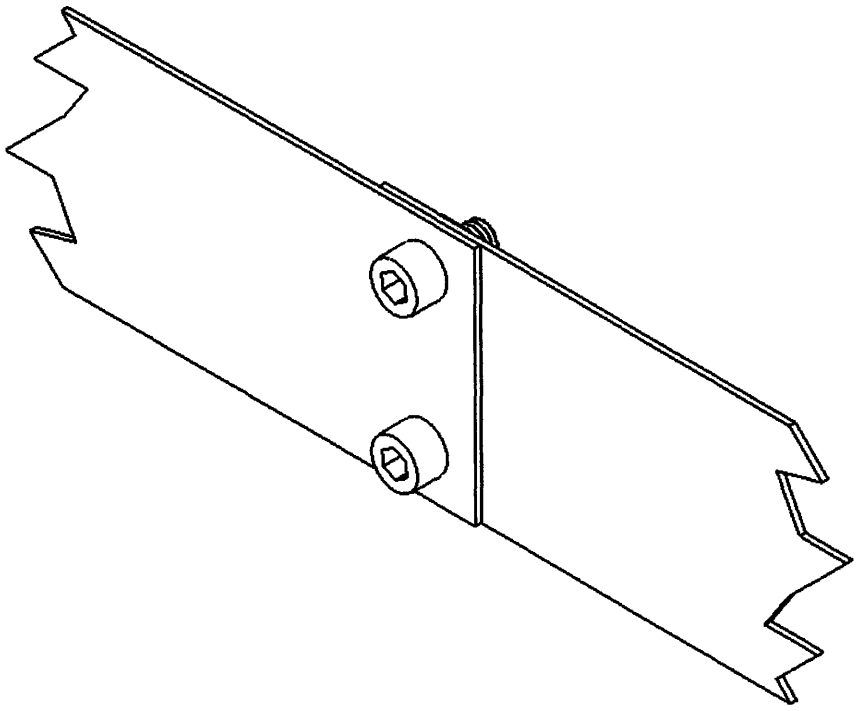

Figure 4.2. Two beams are jointed by a pair of socket cap screws.

The mass of the two additional screws and nuts adds approximately 4 grams to the beam. Compared to each 1.5 meter aluminum segment, which has a mass of approximately 100 grams, this is an insignificant increase.

4.2 Gripper Design

The gripper design which was implemented has two main components. Figure 4.3 shows the final design chosen for the gripping joint.

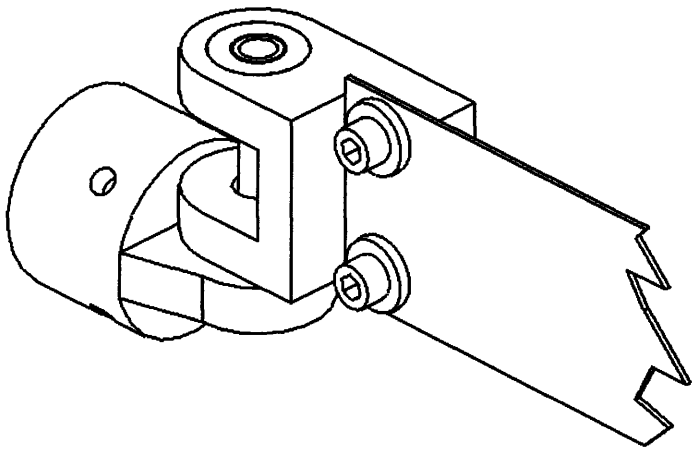

Figure 4.3 Gripping joint mechanism.

The wrist piece and hand piece described earlier in Figure 3.8 are still the main components in the final design. The thumb piece, however, has been replaced with two washers. These washers help distribute the clamping forces of the screws across the surface of the flexible beam.

4.2.1 Wrist piece

The wrist piece is cut out of one inch diameter ABS plastic, and attaches to the existing stainless steel tube which forms the forearm of the robot. The wrist piece fits within the inner diameter of the tube, and is held in place by four 4-40 screws, as shown in Figure 4.4.

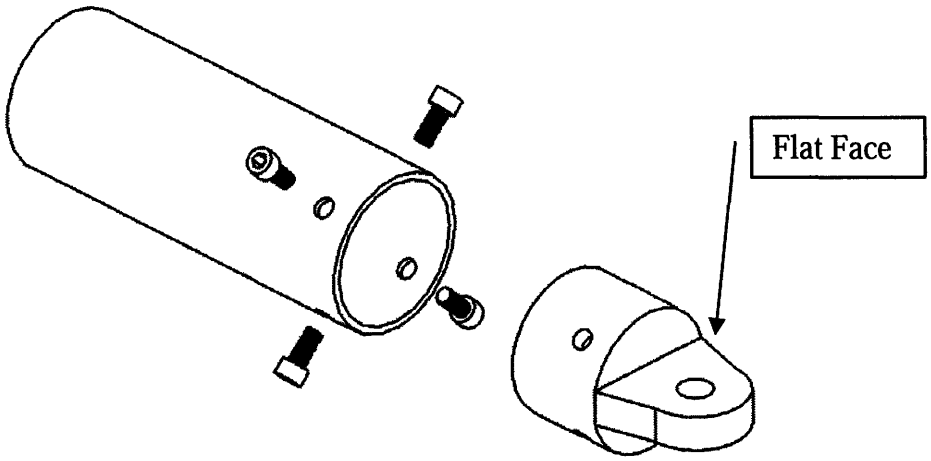

Figure 4.4 Assembly of a hand piece with the robot end of the robot manipulator.

The wrist piece also has a flat face, which has a single hole cut through it. This face is parallel to the ground plane, and the hole is sized such that a ¼ inch shaft can be pressed into it. This ¼ inch shaft serves as the axis of rotation for the pin joint between the robot manipulator and the beam. The ¼ inch shaft is shouldered, so that bearings can rest on the shoulder, without rubbing against the flat surface, as shown in Figure 4.5.

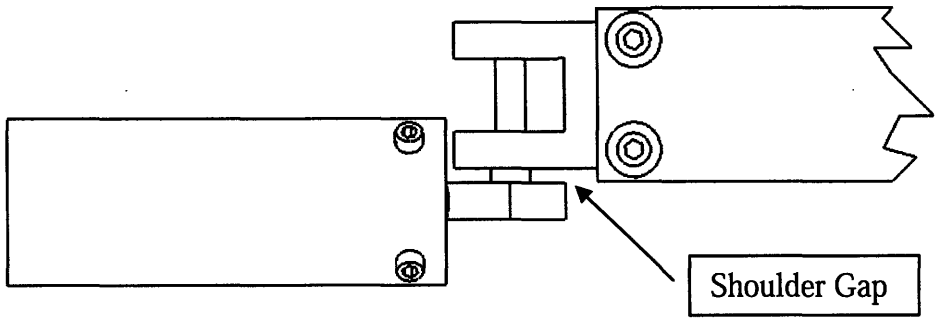

Figure 4.5 A side view of the gripper: the shouldered rod keeps two surfaces from making contact.

4.2.2 Hand Piece

The hand piece has had several changes since the first design detailed in Section 3.6.2. Most notably, a second bearing has been added. Figure 4.6 shows an earlier design next to the final design.

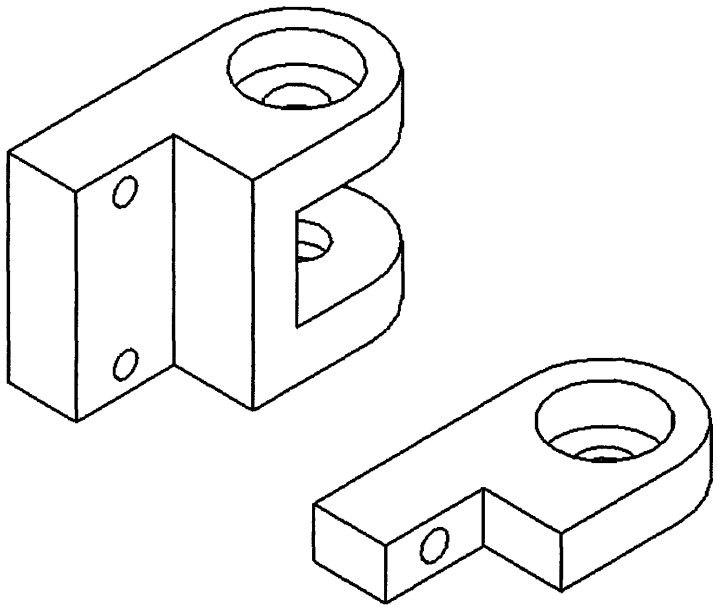

Figure 4.6 A comparison between an earlier design (right) and final design (left) of the hand piece.

The hand is constructed out of a single piece of high density polyethylene. Any lightweight plastic with dimensional stability could have been used, however HDPE was chosen because it was readily available in thick slabs.

The hand piece contains a vertical flat section with two tapped holes for 8-32 screws. These are used to attach the flexible beam, as seen in Figure 4.7.

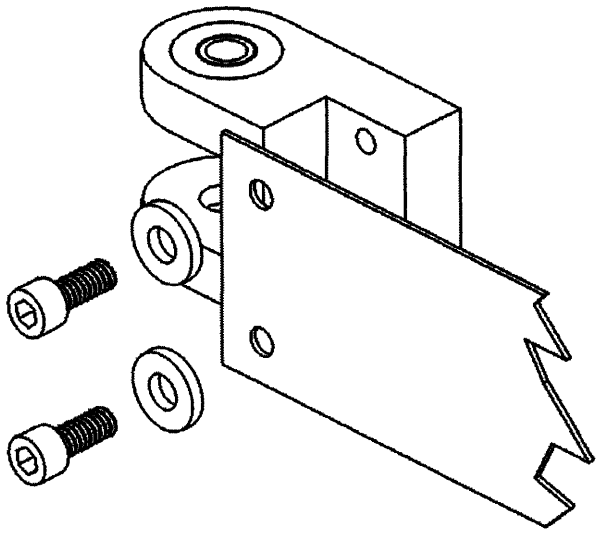

Figure 4.7. Assembly of the flexible beam with the hand piece.

The hand piece also has a pair of counter-bored coaxial holes. Each of these holds has a delrin ball bearing press-fit inside. A clearance hole passes through both counter-bores, allowing for a shaft to pass through both bearings. The assembly of the hand piece with bearings and shouldered rod can be seen in Figure 4.8.

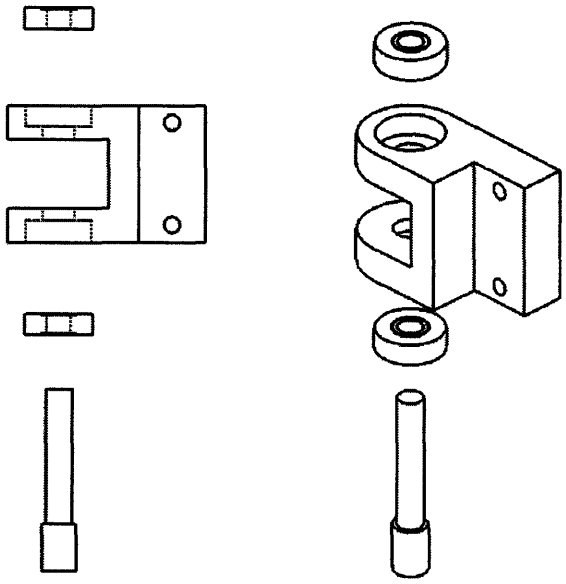

Figure 4.8. Assembly of the bearings, shouldered rod, and hand piece.

The weight of the beam is supported by the hand piece, which is transmitted to the shouldered rod. The load passes through the lower ball bearing as a thrust load. This force is small enough that it does not interfere with the bearing's normal rotation. The bearings used are 3/16" ID delrin bearings. These were selected because they are light weight, low friction, and do not require lubrication.

The addition of a second bearing increases the stiffness of the pin joint against out-of-plane moments, as shown in Figure 4.9.

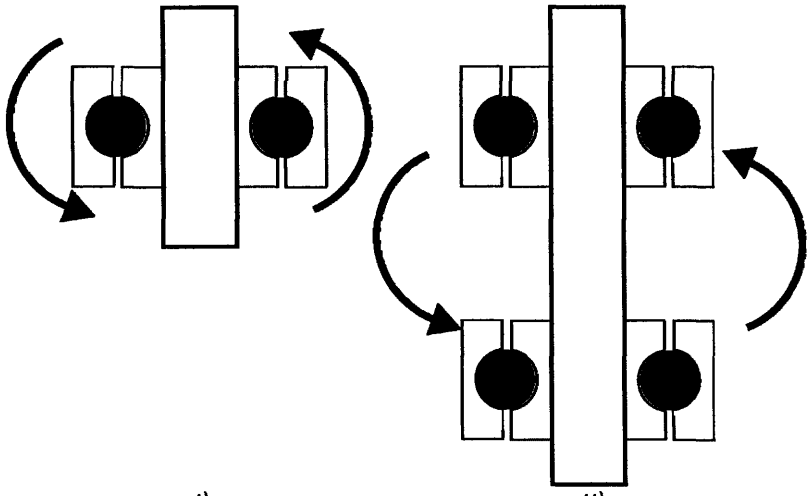

Figure 4.9 Cross section of the pin and bearings. In fig. i) in earlier designs, a single ball bearing does not properly constrain a moment. In fig. ii), the addition of a second bearing greatly increases moment stiffness.

4.3 Passive Floating Modules

The passive floating modules mentioned in Section 3.1 required modifications to be used as a center mass on a beam, or as a passive joint for the assembly experiment. Both attach to the beam, but in different locations, and serving different purposes.

4.3.1 Transportation Experiment

For the transportation experiment, the passive floating module must be secured to the center of the flexible beam. This is accomplished by a clamp mechanism. The clamp mechanism consists of two parallel plates and two screws which can be tightened around the beam, as shown in Figure 4.10.

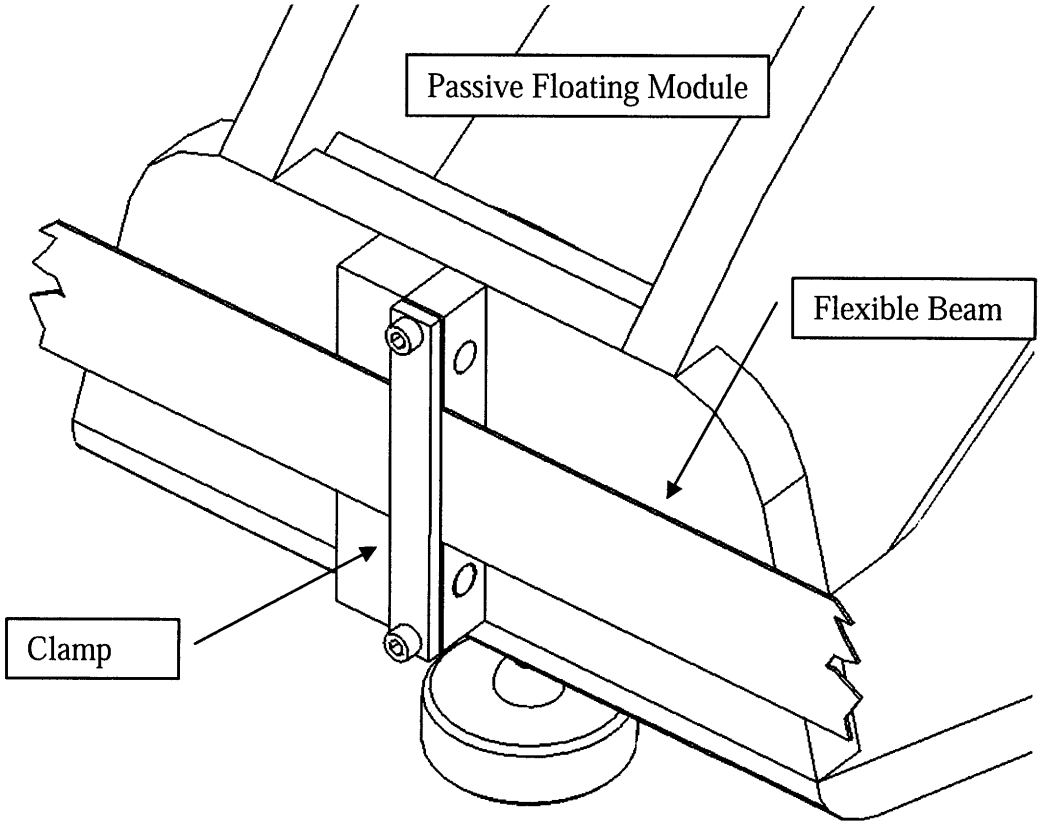

Figure 4.10. A clamp that attaches a passive floating module to the center of a flexible beam.

The clamping mechanism is attached to the passive floating module by two screws. Two tapped holes in the clamp align with two clearance holes in the passive floating module. This assembly is shown in Figure 4.11.

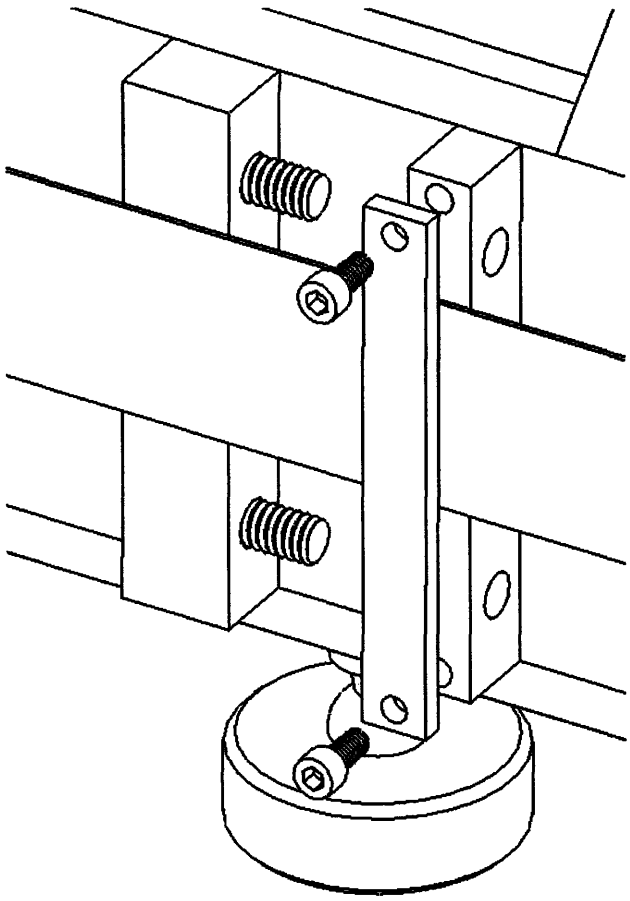

Figure 4.11. Screws attach the clamp to the passive floating module.

4.3.2 Assembly Experiment

For the assembly experiment, two beams ends must be supported by a passive floating module. Ideally, these would both attach at the center of mass of the floating module, so that no rotational inertia from the module would transfer to the beam. Unfortunately, the design of the existing floating module places center of mass inside of the pressurized CO_2 canister. Since this is not possible location to attach the flexible beams, the beams are mounted on vertical rods attached at the front of the floating module. These vertical rods attach to the floating module through the same screw

method as in Section 4.3.1. Figure 4.12 shows the mounting bracket for supporting two beam ends on a floating module.

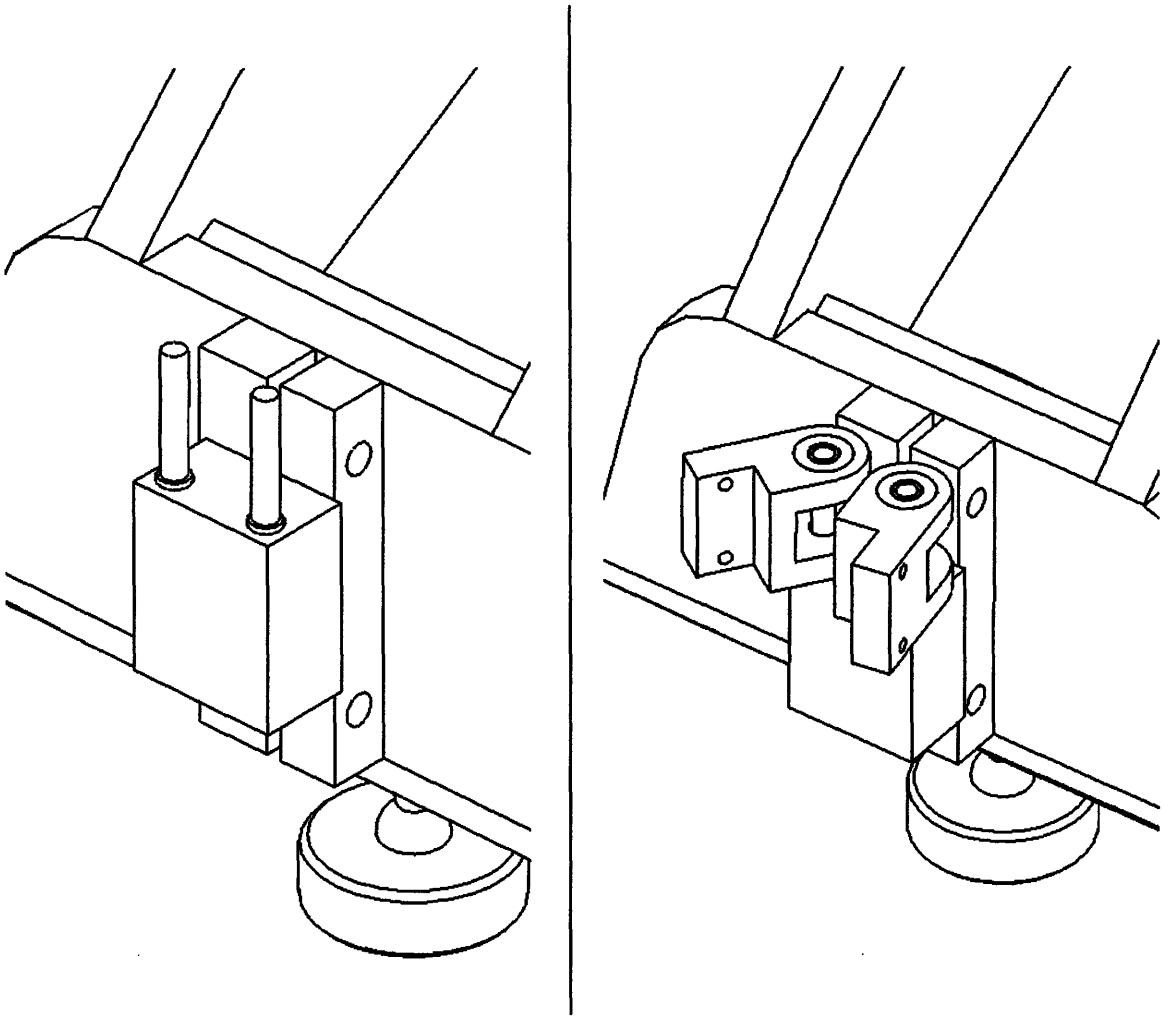

Figure 4.12. Two pins attached to the front of a passive floating module can support the ends of two beams.

The rods are placed as close together as clearance allows, so that small axial forces on the beams do not cause a large rotation of the passive floating module.

CHAPTER

5

CONCLUSIONS

5.1 Contributions of This Thesis

This thesis presented a design to experimentally demonstrate the scaled dynamics of a large flexible beam on-orbit. It also presents the design of a gripping mechanism to support that flexible beam. This design can be used in conjunction with a team of assembly robots to test and verify control algorithms for transportation and assembly of flexible beam structures.

Analysis of various beam compositions and geometries was performed by using a Lagrangian model. This analysis led to the choice of an aluminum beam with cross-section 0.76mm thick and 30 mm tall. The length of the beam depends on which experiment it is being used in.

A gripping mechanism was required to connect the beam to the arms of the robots. The mechanism consists of a pair of ball bearings and a vertically-oriented rod, to create a low-friction pin joint at the end of each manipulator arm. This allows rotation of the joint in the plane of the table, while remaining stiff in all other degrees of freedom.

For the assembly experiments, the flexible modules are arranged into a polygon, with each beam vertex supported by a robot manipulator or by a passive floating module. For the transportation experiment, a single beam is supported at both ends by a robot. In the center of the beam, a floating module is attached.

5.2 Suggestions for Future Work

One of the limiting factors on the maximum length possible for the flexible assembly was torsional stiffness. By decreasing the thickness of the beams, a low natural frequency was reached. However, as the beam's thickness decreased, it became more susceptible to significant amounts of sagging. By using a beam which has a cross section that focuses its mass to the top and bottom extremities, a more torsionally stiff beam might be constructed. This area of beam design was not explored in this thesis due to limitations in the manufacturing process.

Constructing robots with stronger arms would allow a heavier beam to be used. A configuration with a more massive beam would more accurately represent the ratio of robot mass to beam mass, as it would be observed in orbit. A more robust arm can also support a heavier gripping mechanism. A gripping mechanism that is less constrained by weight limitations could be machined out of a more dimensionally stable material, such as aluminum, and utilize a higher precision set of bearings. This might further prevent sag, and allow for longer flexible beams to be tested, which is closer to a full scale representation.

REFERENCES

1 Bilton, A, "Fusion of Remote Vision and On-Board Acceleration Data for the Vibration Estimation of Large Space Structures." MS Thesis, Department of Aeronautics and Astronautics, MIT, 2006.

2 *International Space Station Major Events FY2005* . International Space Station, NASA, 2005. http://www.nasa.gov/pdf/55411main_28%20ISS.pdf

3 Ishijima, Y., Tzeranis, D., and Dubowsky, S. "On-Orbit Maneuvering of Large Space Flexible Structures by Free-Flying Robots." *Proceedings of the 8th International Symposium on Artificial Intelligence, Robotics and Automation in Space, i-SAIRAS*, Munich, Germany, September 2005.

4 Lichter, M. D. "Shape, Motion, and Inertial Parameter Extimation of Space Objects using Teams of Cooperative Vision Sensors," Ph.D. Thesis, Department of Mechanical Engineering, Massachusetts Institute of Technology, Cambridge, Massachusetts, 2004.

5 *Massive Lockheed Martin-Built Solar Arrays to be Launched to International Space Station.* Lockheed Martin, Aug 1, 2006. http://www.lockheedmartin.com/wms/findPage.do?dsp=fec&ci=17849&rsbci=0&fti=0&ti=0&sc=400

6 Meirovitch, L. *Elements of Vibration Analysis.* New York: McGraw-Hill, 1975.

7 Mangalgiri, V. "Analysis for the Robotic Assembly of Large Flexible Space Structures." Master's Thesis, Department of Mechanical Engineering, Massachusetts Institute of Technology, Cambridge, Massachusetts, 2004.

8 *NASA Human Space Flight, Space Station Gallery.* http://spaceflight.nasa.gov/gallery/images/station/index.html.

9 Oberg, James. "International Space Station." World Book Online Reference Center. 2005. World Book, Inc. http://www.worldbookonline.com/wb/Article?id=ar279523.

10 Piedboeuf, J.-C., and É. Dupuis. "Recent Canadian Activities in Space Automation & Robotics – An Overview." *Proceedings of the 7th International Symposium on Artificial Intelligence, Robotics, and Automation in Space: i-SAIRAS 2003*, NARA, Japan, May 2003.

11 Staritz, P.J., S. Skaff, C. Urmson, and W. Whittaker. "Skyworker: A Robot for Assembly, Inspection and Maintenance of Large Scale Orbital Facilities." *Proceedings of the 2001 IEEE International Conference on Robotics and Automation (ICRA 2001)*, Seoul, Korea, pp. 4180-4185, May 2001.

12 Tzeranis, D., Ishijima, Y., and Dubowsky, S. "Manipulation of Large Flexible Structural Modules by Robots Mounted on Large Flexible Structures." *Proceedings of the 8th International Symposium on Artificial Intelligence, Robotics and Automation in Space, i-SAIRAS*, Munich, Germany, September 2005.

13 Ueno, H., T. Nishimaki, M. Oda, and N. Inaba. "Autonomous Cooperative Robots for Space Structure Assembly and Maintenance." *Proceedings of the 7th International Symposium on Artificial Intelligence, Robotics, and Automation in Space: i-SAIRAS 2003*, NARA, Japan, May 2003.

APPENDIX

A

DIMENSIONED PART DRAWINGS

A.1 Wrist Piece

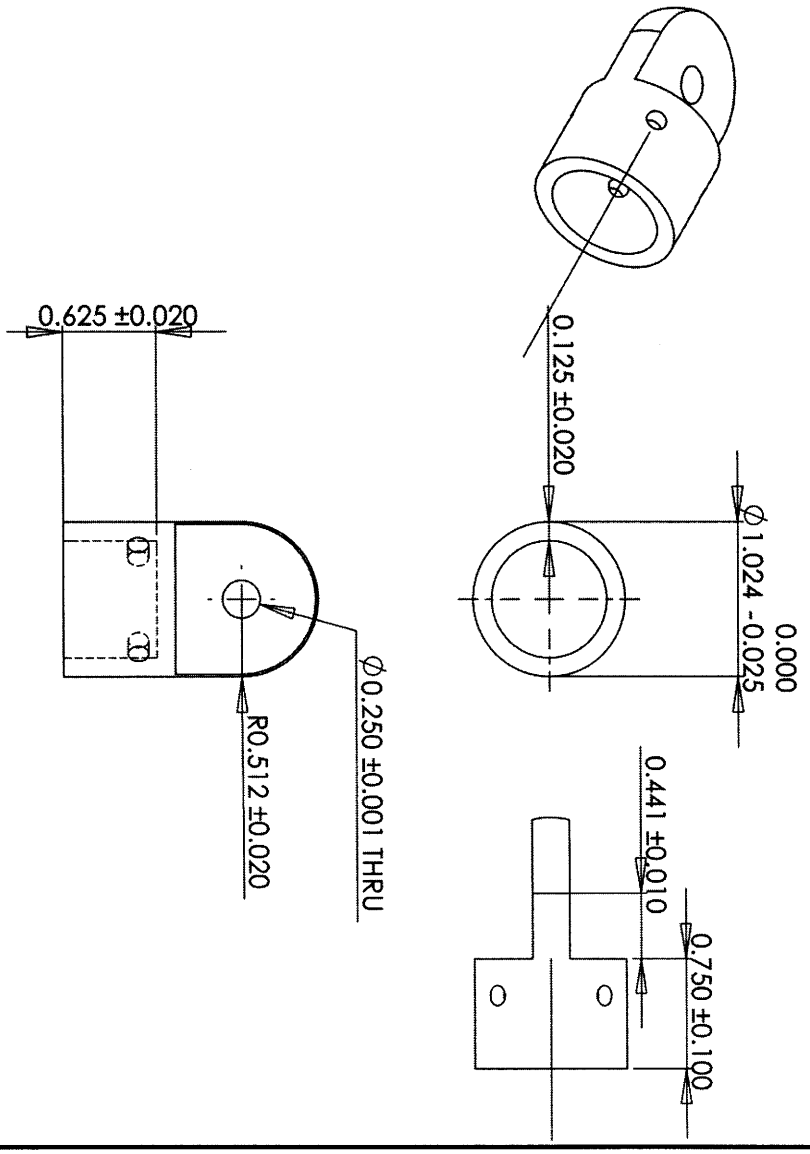

A.2 Hand Piece

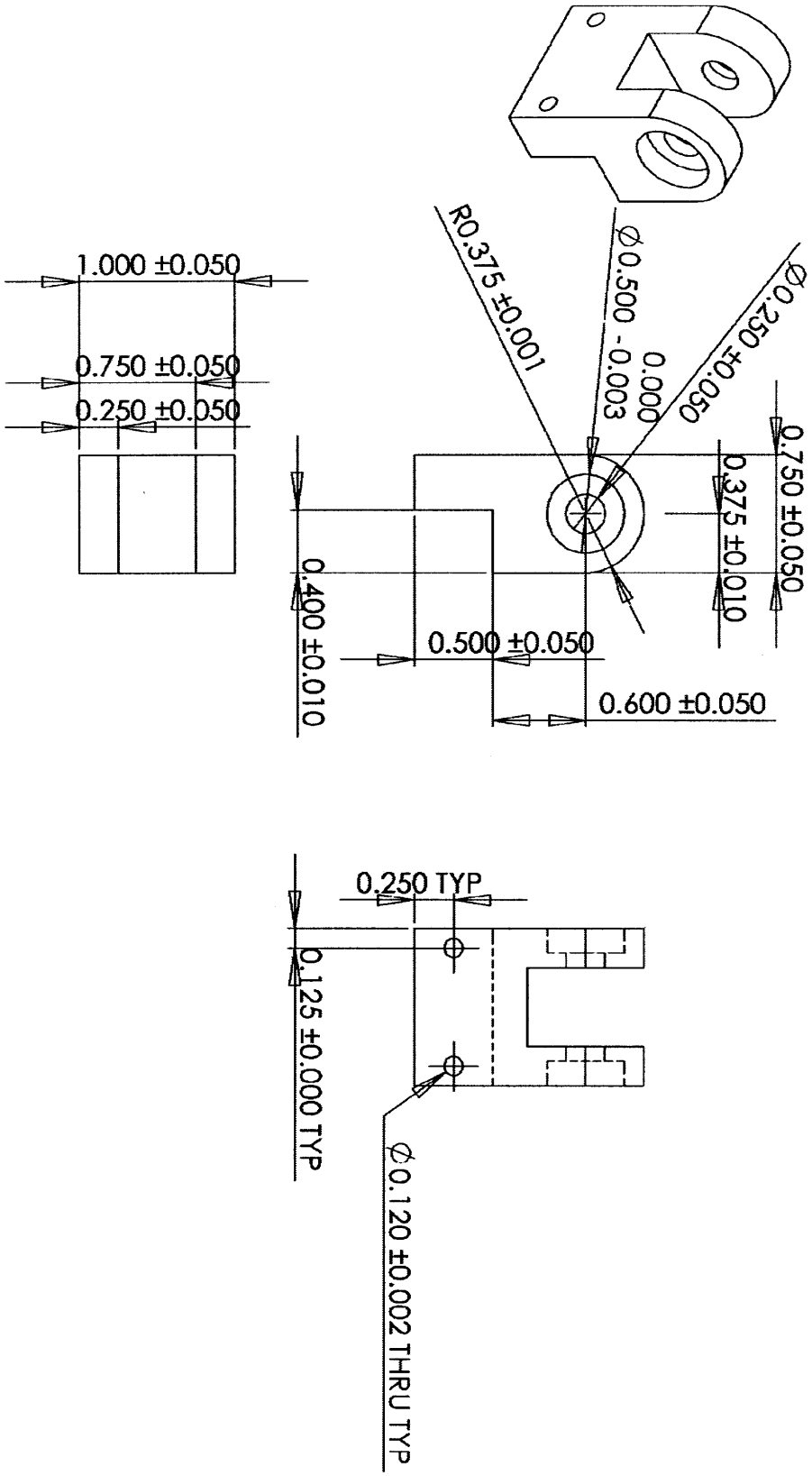

APPENDIX

B

PHOTOGRAPHS

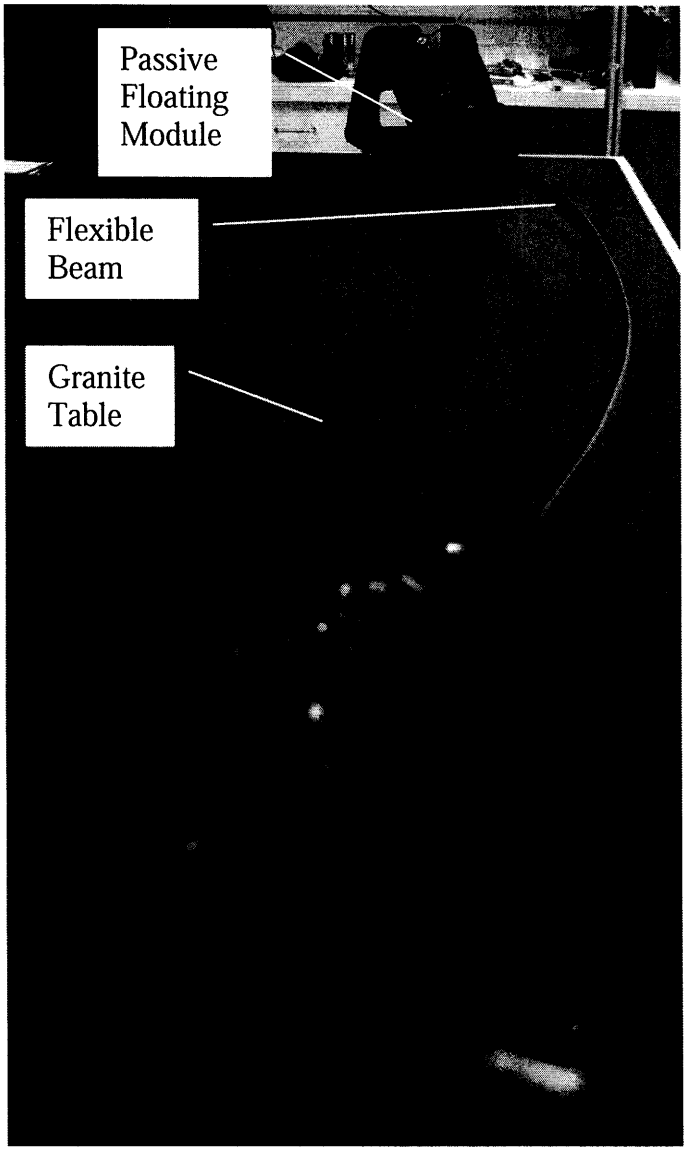

Figure B.1. Test assembly displaying a large beam displacement.

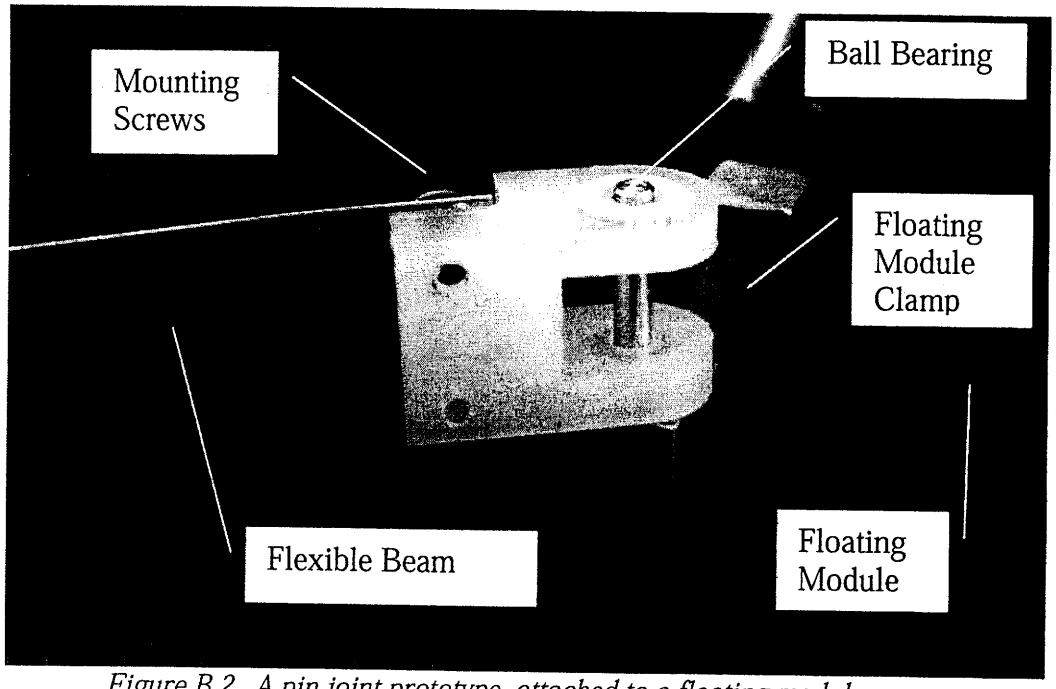

Figure B.2. A pin joint prototype, attached to a floating module.

Figure B.3. An early-stage prototype, with only one bearing.